Posted on 24 Nov 2022 — The copyright holder is the author/funder. All rights reserved. No reuse without permission. — https://doi.org/10.1002/essoar.10501004.1 — This a preprint and has not been peer reviewed. Data may be preliminary.

Geomagnetic activity control of irregularities occurrences over the crests and trough of the African EIA

Paul, Obiakara Amaechi[1], Elijah, Oyedola Oyeyemi[2], Andrew, Oke-Ovie Akala[2], and Christine Amory-Mazaudier[3]

[1]Chrisland University
[2]University of Lagos
[3]University Pierre and Marie Curie

November 24, 2022

Abstract

This paper examined the behavior of ionospheric irregularities over the African Equatorial Ionization Anomaly (EIA) during intense geomagnetic storms which occurred from 2012 to 2015. Total electron content (TEC) data was used to derive the rate of change of TEC index (ROTI). This was employed to monitor irregularities over the trough and crests of the EIA. Variations of the horizontal component of the Earth's magnetic field (H) were examined. The H component was additionally used to compute ionospheric electric current disturbance (Diono). Prompt penetration electric field (PPEF) inferred from variations of Diono was compared with PPEF obtained from the Prompt Penetration Equatorial Electric Field Model (PPEFM). The PPEFM predicted accurately all PPEFs thus, was found to be valid over the African EIA. The local time of occurrence of interplanetary magnetic field (IMF) dictated the behavior of irregularities. Eastward PPEF triggered short duration irregularities on 23 April 2012, 17 March 2013 and 20 February 2014 while westward disturbance dynamo electric field (DDEF) reduced them thereafter. During the storms recovery including the 15 July 2012 and 17 March 2015 events, irregularities were suppressed by westward DDEF. However, during the storms of 14 November 2012 and 29 June 2013 no irregularities were observed. Irregularities were always inhibited over the trough. The inhibition lasted longer during the super storm of March 2015. Over the crests, there were differences in their behavior on 16-17 July 2012, 15 November 2012 and 19 March 2013. These were however, not linked to storm-time electric field.

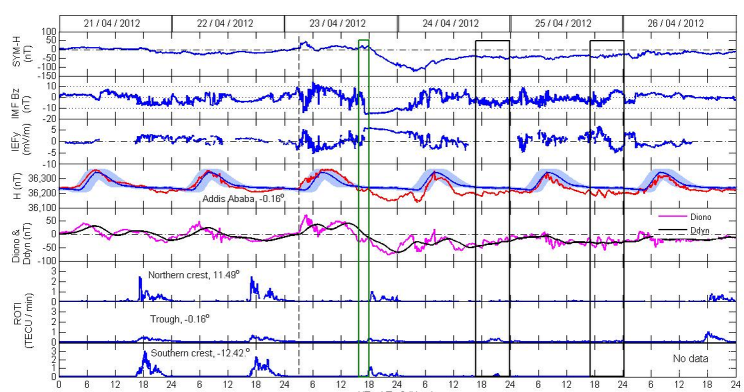

Posted on 24 Nov 2022 — The copyright holder is the author/funder. All rights reserved. No reuse without permission. — https://doi.org/10.1002/essoar.10501004.1 — This a preprint and has not been peer reviewed. Data may be preliminary.

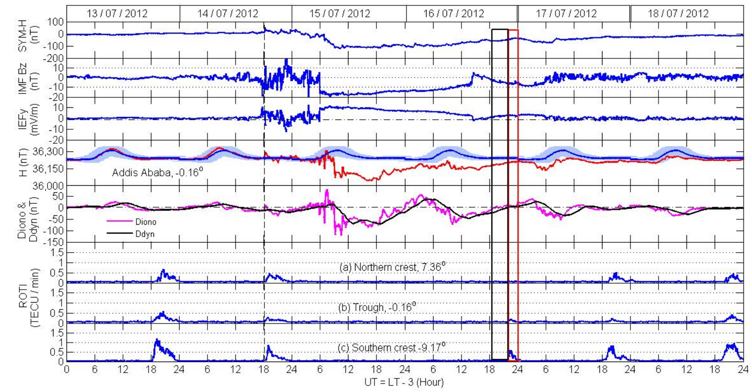

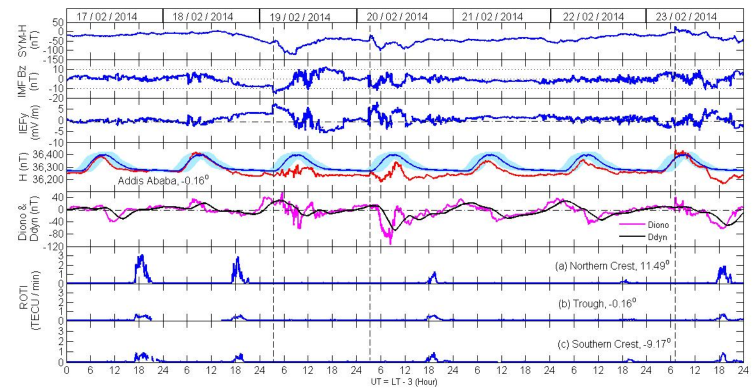

Geomagnetic activity control of irregularities occurrences over the crests and trough of the African EIA

P. O. Amaechi[1, 2], E. O. Oyeyemi[2], A. O. Akala[2, 3, 4, 5], C. Amory-Mazaudier[6, 7]
[1]Department of Physical Sciences, Chrisland University, Owode, Abeokuta
[2]Department of Physics, University of Lagos, Yaba, Lagos, Nigeria
[3]Distance Learning Institute, University of Lagos, Akoka, Yaba, Lagos, Nigeria
[4]Maritime Institute, University of Lagos, Akoka, Yaba, Lagos, Nigeria
[5]The Abdus Salam International Centre for Theoretical Physics, Trieste, Italy
[6]Sorbonne Universités, LPP, Polytechnique, Paris, France
[7]T/ICT4D, ICTP,Trieste Italy

Corresponding author: Paul Amaechi (paoloobiaks@yahoo.fr)

Key points:

- Combined effect of PPEF and DDEF on ionospheric irregularities over the crests and trough of the Africa EIA during intense storms.
- Differences in irregularities behaviour over the crests of the African EIA unrelated to geomagnetic storms during the recovery phase.
- Validation of the Prompt Penetration Equatorial Electric Field Model over the Africa sector during the main phase of intense storms.

Abstract

This paper examined the behavior of ionospheric irregularities over the African Equatorial Ionization Anomaly (EIA) during intense geomagnetic storms which occurred from 2012 to 2015. Total electron content (TEC) data was used to derive the rate of change of TEC index (ROTI). This was employed to monitor irregularities over the trough and crests of the EIA. Variations of the horizontal component of the Earth's magnetic field (H) were examined. The H component was additionally used to compute ionospheric electric current disturbance (Diono). Prompt penetration electric field (PPEF) inferred from variations of Diono was compared with PPEF obtained from the Prompt Penetration Equatorial Electric Field Model (PPEFM). The PPEFM predicted accurately all PPEFs thus, was found to be valid over the African EIA. The local time of occurrence of interplanetary magnetic field (IMF *Bz*) dictated the behavior of irregularities. Eastward PPEF triggered short duration irregularities on 23 April 2012, 17 March 2013 and 20 February 2014 while westward disturbance dynamo electric field (DDEF) reduced

them thereafter. During the storms recovery including the 15 July 2012 and 17 March 2015 events, irregularities were suppressed by westward DDEF. However, during the storms of 14 November 2012 and 29 June 2013 no irregularities were observed. Irregularities were always inhibited over the trough. The inhibition lasted longer during the super storm of March 2015. Over the crests, there were differences in their behavior on 16-17 July 2012, 15 November 2012 and 19 March 2013. These were however, not linked to storm-time electric field.

1. Introduction

Ionospheric irregularities are small to large-scale structures that form in the plasma density [*Pekins, 1975*]. Their interaction with Global Navigation Satellite System (GNSS) signals could result in rapid fluctuations in the amplitude and/or phase fluctuation of the signals, giving rise to a phenomenon known as scintillations [*Aarons,* 1982*; Datta-Barua et al.,* 2015]. During intense scintillation conditions, GNSS signals might suffer degradation, reduction in their information content or failure in reception [*Aarons et al.*, 1996*; Kintner et al.*, 2007]. The outcome could have disastrous effect on the life-critical GNSS applications especially, those utilized in navigation, positioning, search and rescue as well as military operations and surveying [*Conker et al.,* 2003*; Sunda et al.,* 2015*; Yizengaw and Groves,* 2018]. For this reason, adequate information about the actual state of the ionosphere is crucial for the smooth operation of the critical GNSS applications during all weather conditions.

The dynamics of the quiescent ionosphere is driven to a large extent by zonal electric field resulting from the dynamo action of neutral wind. The electric field which is eastward during the day and westward a night controls the distribution of ionization especially, over the equatorial/low latitude region [*Fejer and Scherliess*, 1997*; Heelis*, 2004; *Fejer et al.*, 2016]. The interaction between eastward electric field and the horizontal north-south geomagnetic field gives rise to the equatorial ionization anomaly (EIA) [*Appleton*, 1946*; Yue et al.,* 2015]. In the post sunset period, the pre reversal enhancement (PRE) in $\boldsymbol{E} \times \boldsymbol{B}$ drift velocities further lifts the ionosphere up [*Fejer et al.*, 1999] to altitude where the development of ionospheric irregularities is favoured through the generalized Rayleigh-Taylor instability (R-T instability) [*Farley et al.,* 1970*; Eccles,* 2004; *Yizengaw et al.,* 2013a]. The plasma bubbles irregularities so developed rise above the magnetic equator, then move along geomagnetic fields towards the crests of the EIA

[*Groves et al.,* 1997]. The salient parameters affecting the generation of irregularities as captured by the equation for the RT instability growth rate [*Kelley,* 1989*; Sultan,* 1996] are the: (i) post sunset vertical drift, (ii) components of thermospheric winds, (iii) density gradient at the bottom side of the F-layer, and (iv) initial seed perturbations due to gravity wave from the lower atmosphere [*Ott,* 1978*; Haerendel,* 1973*; Kudeki et al.,* 2007*; Tsunoda et al.,* 2013].

During solar disturbances such as geomagnetic storm, electrodynamics of the equatorial/low latitude ionosphere undergoes drastic and unpredicted variations. Generally, when the z-component of the interplanetary magnetic field (IMF *Bz*) turns south and auroral currents intensify, magnetospheric convection electric field penetrate promptly into the low-latitude ionosphere in the form of an under-shielding electric field, the so-called dawn-to-dusk prompt penetration electric field (PPEF) [*Kikuchi et al.,* 2008*; Abdu,* 2012*; Abdu et al.,* 2018]. However, the shielding layer provided by the subsequent development of region 2 field aligned current (R2-FAC) at timescales of 20-30 minutes under northward turning of IMF *Bz* and corresponding decrease in convection activity attempts to balance the convection electric field. This gives rise to the penetration of an over-shielding dusk-to-dawn electric field to the equatorial region [*Abdu et al.,* 2018]. On the other hand, Joule heating of the thermosphere resulting from the excessive input of energy at high latitude during the disturbance drives meridional winds which in turn travel down to the equatorial region, generating disturbance dynamo electric field (DDEF). The simulation of the global dynamo effect of these winds was first performed by *Blanc and Richmond* [1980]. It has been reported that this type of disturbance take about 4-5 hours to reach the low-latitude depending on their speed [*Fuller-Rowell et al.,* 1997] while their ensuing effects are known to last longer during the recovery phase of geomagnetic storms [*Scherliess and Fejer,* 1997].

Chapman [1919] was the first to show that during intense geomagnetic disturbances, the horizontal component of the geomagnetic field (H) measured using ground magnetometers reduces significantly below its average behavior. Later on, *Nishida et al.* [1966] identified disturbance polar no. 2 (DP2) as the geomagnetic counterpart of convection electric field generated by the interaction of the solar wind and the magnetosphere. *Nishida* [1968] further found that DP2 fluctuations observed in ground magnetic measurements were consistent with interplanetary magnetic field data. *Vasyliunas* [1970] formulated a theoretical model for magnetospheric convection while model results of *Fejer and Scherliess* [1997] showed that the PPEF vanished after 60 minutes due to the shielding effect of the ring current. *Manoj et al.* [2008] observed that the maximum propagation time for interplanetary electric field (IEF) to travel from the nose of the bow-shock nose to the equatorial ionosphere is 17 minutes while the coherence between IEF and equatorial electric field (EEF) peaks around 2 hours period and increases during period of magnetic activity. According to *Le Huy and Amory-Mazaudier* [2005, 2008] the magnetic signatures of the reversed solar quiet (Sq) current at low latitude during magnetic storms are due to the ionospheric disturbance dynamo (Ddyn) which is the equivalent current system associated to DDEF. The characteristics of DP2 and Ddyn have been summarized in terms of their period, ionospheric responses and source/origin [*Amory-Mazaudier et al.,* 2017].

The time of occurrence of disturbed electric field is crucial in affecting the behaviour of irregularities. PPEF of eastward polarity occurring in the post sunset period can enhance the ambient eastward PRE thus, triggering irregularities or enhancing them. Conversely, westward PPEF/ DDEF can reduced or inhibit the formation of irregularities. Despite its wider spatial coverage over the low-latitude region, Africa has the fewer number of studies in terms of ionospheric response to storm-time electric fields. The lack of studies for Africa has been attributed to the long time absence of ionospheric observational tools over this sector [*Paznukhov et al.,* 2012; *Yizengaw et al.,* 2013b]. This in turn constitutes an impediment to global modeling. Over the last decade, the availability of ground-based instruments thanks to projects such as the International Equatorial Electrojet Year (IEEY), the International Heliophysical Year (IHY) and the International Space Weather Initiative (ISWI) has help in improving the knowledge of the peculiar features of the ionosphere over Africa.

For example, evidence of the inhibition/development of the PRE by storm time electric field was presented by *Ngwira et al*. [2013] during the storm of 6/8 April 2011 using the Communication/Navigation Outage Forecasting System (C/NOFS) satellite data. Consequently, larger depletion in TEC and electron density as well as enhanced scintillations were respectively, absent and present in Nairobi, Kenya and Kampala, Uganda on these days. In addition, *Azzouzi et al*. [2015] observed that the geomagnetic storm had no effect on irregularities on 2 October while it inhibited them on 8 and 30 October over East Africa as well as over the entire continent on 14 October. They found no increase in the virtual height of the F2 layer (hoF2) at Ascension

Island suggesting that PRE was absent on 14 October along with the presence of westward DDEF which also acted to inhibit the regular eastward electric field. Their study further revealed an asymmetry in irregularities as captured by the rate of change of TEC index (ROTI) over East and West Africa during the storms of October 2013.

Also, *Fathy et al.* [2014] separated Ddyn associated with DDEF from DP2 related to PPEF and observed a reduction in H during four consecutive days as a result of the presence of Ddyn. They postulated that the main component of Ddyn is a diurnal oscillation which varied from the Europe-African, to the Asian and then American longitudes with the strongest Ddyn effect registered over the African longitude during the storm of 5 April 2010. Similarly, *Nava et al.* [2016] isolated DP2 and Ddyn signals from the ionospheric electric current disturbance (Diono) during the St. Patrick day storm of 17 March 2015. They confirmed that short term oscillations of about 3 h periods were related to DP2 fluctuations during period of southward IMF *Bz* and occurred simultaneously in the Asian, African, and American sectors while Ddyn showed difference related to the local time of each sector and lasted longer over the Asian then African and finally American sectors. They finally detected the presence of planetary waves with period of 5 and 9 days originating from the lower atmosphere using wavelet analysis.

In the same vein, *Zaourar et al.* [2017] observed larger disturbances in amplitude of Ddyn in the northern hemisphere than in the southern hemisphere, and stronger asymmetries at higher latitudes, than at lower latitudes, between conjugate observatories. At equatorial and low latitudes they found that Diono was more intense over the American sector than the African sector while Ddyn lasted longer (4 days) in the later sector than the earlier (2 days). They also stressed on changes in the amplitude of the magnetic perturbations which exhibited a gradual decay towards lower latitudes. *Amaechi et al.* [2018a] studied the effect of storms on ionospheric irregularities over the eastern and western African sector in the year 2015. They observed fluctuation in H and minima/oscillations in Diono over magnetometers in both sectors associated with PPEF during the main phase. The separation of the effect of DP2 from Ddyn revealed the presence of westward DDEF several hours after the beginning of the disturbance. The westward electric field inhibited irregularities during the main phase of March and October 2015 events while eastward electric field triggered them over the eastern sector during the June 2015 storm. During the recovery phase, westward DDEF suppressed irregularities. Their study revealed a longitudinal difference in the pattern of irregularities between the Eastern and Western African sectors during the recovery phases of the storms of March and October 2015.

There has also been modeling efforts aimed at assessing the ability of storm to both enhance and suppress irregularities. For instance *Carter et al.* [2014] obtained good correspondence between the R-T growth rate estimated using the Thermosphere-Ionosphere- Electrodynamics General Circulation Model (TIEGCM) and Equatorial Plasma Bubbles (EPBs) occurrence over the American (289.59^{o}E), Atlantic (345.59^{o}E), Eastern African (36.81^{o}E), Asian (88.37^{o}E) and Eastern pacific (144.87^{o}E) longitudes. They also observed that for longitude where EPBs occurrence maximizes during equinox, the TIEGM gave an accurate representation of the decreased in PRE and associated inhibition of irregularities growth rate on days when EPBs were absent. They further found a decrease in the modeled values of the linear R-T growth during periods of increased Kp activity. *Nayak et al.* [2016] demonstrated the ability of the Prompt Penetration Electric Field Model (PPEFM) in predicting PPEF and the corresponding effect on irregularities in the Asian sector during the storm of 17 March. Such modeling studies are more than ever needed over the African EIA during storms.

Despite all these works, a better understanding of the storm-time behaviour of ionospheric irregularities is still needed over the African EIA. Features such as the simultaneous response of ionospheric irregularities to PPEF, DDEF and the combination of both disturbed electric field over the crests and trough of the African EIA, as well as the asymmetry trend of irregularities occurrences over the EIA crests in both hemispheres are yet to be investigated during various storms. This poses not only a limitation to global modelling but also challenge to forecasting space weather which has long been the goal of the Space Physics and Aeronomy (SPA) community. This is all the more pertinent given the fact that ionospheric response to geomagnetic storm can be highly localized and can vary significantly from one storm to another [*Kakad et al.*, 2012; *Nayak et al.,* 2016]. This paper thus, focused on the simultaneous variations of irregularities over the crests and trough of the African EIA during intense geomagnetic storms of the ascending phase of solar cycle 24. The study further performed for the first time over the African EIA region, comparison between PPEFs derived from ground based magnetometer data and inferred from the PPEFM [*Manoj and Maus,* 2012]. The careful selection of storm events with different intensity, time of Sudden Storm Commencement (SSC), season of occurrence, duration of the main phase, duration and strength of southward IMF *Bz,* offered an unprecedented scenario to examine variations of DP2 and Ddyn current systems in conjunction with their modulating effect in the post sunset ionosphere over the least studied African sector during intense geomagnetic disturbances. To this end, section 2 describes the data sets and method of analysis while section 3 gives a highlight of the results obtained. The discussion and conclusion are presented in section 4 and 5, respectively.

2. Data sets and Data Processing

2.1 Data sets

All storm events were associated with Coronal Mass Ejection (CME) [see the Solar and Heliospheric Observatory (SOHO)/Large Angle and Spectrometric Coronagraph (LASCO) CME Catalogue at https://cdaw.gsfc.nasa.gov/CME_list/ for a description of basic attributes of the events]. Their evolution in the interplanetary medium was monitored using interplanetary parameters mainly IMF *Bz* and the x component of the solar wind speed (Vx). The corresponding effect in the Earth's magnetosphere was examined with the symmetric H index (SYM-H) as well as the north component (X) and the east component (Y) of the geomagnetic field. The ionospheric response vis-à-vis irregularities variation was analyzed using indices derived from GNSS observables in addition to ground based magnetometer data.

SYM-H data are provided by the International Service of Geomagnetic Indices (ISGI) at htpp://isgi.unistra.fr. This data set with 1 minute resolution is more suitable for monitoring changes in the solar wind dynamic pressure [*Wanliss and Showalter,* 2006] and related current in the magnetosphere during storms. It was also used to capture the SSC and indicate the time of arrival of the CME shock on the magnetosphere [*Azzouzi et al.,* 2015]. IMF *Bz* and Vx data with time resolution of 64 seconds are recorded on board the Advanced Composition Explorer (ACE) satellite. These data are in Geocentric Solar Magnetospheric (GSM) coordinates where the x-axis is positive sunward. They were retrieved from http://www.srl.caltech.edu/ACE/ASC/level2/mag-_12desc.html and time shifted by about 52 minutes to account for propagation delays to the Earth's magnetosphere [*Chakrabarty et al.,* 2005]. IMF *Bz* and Vx were thus, utilized to compute the y-component of interplanetary electric field otherwise known as convection electric field (IEFy).

The Earth's magnetic field data from the magnetometers at the Addis Ababa station was employed. This magnetometer is managed by the Institut de Physique du Globe de Paris (IPGP) while data are distributed via the International Real-Time Magnetic Observatory Network (INTERMAGNET) at www.intermagnet.com. These data were used to compute the horizontal component of the Earth's magnetic field (H). The coordinates and location of the magnetometer station are given in Table 1 and Figure 1 respectively. GNSS observables for stations located in the African equatorial/low-latitude region around longitude 30^{o}E were obtained from University NAVSTAR Consortium (UNAVCO) at htpp://www.unavco.org/data/data.html. These data with resolution of 30 minutes were used to estimate vertical TEC (VTEC) and derive the rate of change of TEC index (ROTI). The coordinates of the GNSS stations are also given in Table 1 and Figure 1 respectively.

2.2 Methods of analysis

Convection electric field (*IEFy*) was estimated using the formula $IEF_y = -V_{\times} \times IMF\ Bz$ [*Kelley*, 1989] while the horizontal component of the Earth's magnetic field (*H*) was computed using $= \sqrt{X^2 + Y^2}$.

According to *Cole* [1966], the observed *H* is a combination of currents systems flowing in the magnetosphere-ionosphere (MI) system. It is given by:

$$H = S_R + D \qquad (1)$$

where S_R is the daily solar regular variation of the Earth's magnetic field associated to the regular ionospheric dynamo due to solar heating [*Mayaud*, 1965] and *D* is the integrated effects of disturbances coming from various current systems flowing in the Magnetosphere –Thermosphere system [*Zaourar et al.*, 2017].

S_R was estimated as the mean of *H* during five most geomagnetically quiet days in each month selected from the GFZ German Research Centre for Geosciences website ftp://ftp.gfz-potsdam.de (Table 2).

$$<H> = \frac{1}{n}\sum_{i=1}^{n} H_i \qquad (2)$$

Neglecting the effect of induced ground currents [*Sabaka et al.,* 2004] as well as Chapman Ferraro currents and the tail currents in the presence of the generally strongest ring current, equation 1 reduces to:

$$H = < H > + DP + Ddyn + SYM\text{-}H \times cos\delta \qquad (3)$$

where $<H>$ is the mean of H during geomagnetic quietest days, $SYM\text{-}H \times cos\delta$ is the symmetric component of the ring current and δ is the geomagnetic latitude of the station. DP is the disturbance polar currents (DP) [*Nishida et al.*, 1966, *Kamide and Fukushima*, 1972] and Ddyn is the ionospheric disturbed dynamo currents [*Blanc and Richmond*, 1980; *Le Huy and Amory-Mazaudier*, 2005; *Fathy et al.,* 2014].

The term DP + Ddyn is known as the ionospheric electric current disturbance (Diono) [*Zaourar et al.,* 2017; *Amory-Mazaudier et al.,* 2017; *Amaechi et al.,* 2018a,b]. Diono combines the effects of: (i) the disturbance polar no.1 (DP1), (ii) disturbance polar no.2 (DP2), (iii) disturbance polar no.3 (DP3) and (iv) disturbance polar no.4 (DP4) as well as ionospheric disturbed dynamo currents (Ddyn) [*Zaourar et al.,* 2017]. DP1 is one cell current system on the nightside associated with substorm [*Rostoker* 1967, 1969] while DP2 is the one expanding from pole to equator due to convection electric field [*Nishida*, 1968]. DP3 is a system of current flowing in the polar cap with direction opposite to that of DP2 [*Kuznetson and Troschichev*, 1977; *Troschichev and Janzhura*, 2012]. The current system of the disturbance related to the azimuthal component of IMF is termed DP4 [*Svalgaard,* 1968; *Kuznetson and Troschichev*, 1977].

DP1, which is on the night side is negligible. Also DP3 and DP4 which are restricted to the polar cap [*Stauning,* 2012] are negligible at middle and low latitude. Based on these considerations Diono reduces to:

$$Diono = DP2 + Ddyn \qquad (4)$$

DP2 is the equivalent current system due to PPEF [*Nishida,* 1968] and Ddyn is the equivalent current system associated to DDEF [*Blanc and Richmond,* 1980]. *Diono* can then be derived as:

$$Diono = H - < H > - SYM\text{-}H \times cos\delta \qquad (5)$$

Short-term oscillations of about 2 hours associated with southward turning of IMF *Bz* are the signature of DP2 [*Nava et al.,* 2016] while diurnal oscillations are attributed to Ddyn [*Le Huy and Amory-Mazaudier,* 2005]. At the equatorial region, Ddyn is absent at the beginning of the storm since it requires several hours to get to the low latitudes. In this situation, DP2 becomes significant and can be approximated to Diono. Similarly, when a magnetic quiet day immediately follows a storm and there is no auroral activity and by implication no convection electric field, DP2 become zero and Ddyn can also be approximated to Diono [*Amory-Mazaudier et al.,* 2017]. Based on these, a running average filter that takes the mean value of 4 hours of Diono data with sliding of 1 hour was used for the separation of Ddyn from DP2 [*Fathy et al.,* 2014; *Azzouzi et al.,* 2015; *Amaechi et al.,* 2018b].

To have further insight into the behavior of PPEF during the main phases of the storm events under consideration, the PPEFM was used to estimate PPEF for the African sector around mean longitude 37^{o}E. This model is mainly a transfer function which models daily variations of equatorial ionospheric electric fields using interplanetary electric field (IEF) data mapped in the solar wind. Details about it can be found in http://geomag.org/models/PPEFM/RealtimeEF.html. The input parameters were time and location while the output parameter was estimated values of equatorial electric field (EEF) mainly (i) the quiet time electric field (background electric field) and (ii) the total electric field (PPEF plus background electric field).

After subjecting GNSS observables to quality check using the Translating Editing and Quality Checking (TEQC) software [*Estey and Meertens,* 1999], relative Slant Total Electron Content (STEC) was estimated by leveling the carrier phase with the pseudorange measurements [*Hansen et al.,* 2000]. Prior to that, eventual cycle slips in the phase data were detected and corrected [*Blewitt,* 1990]. Absolute STEC was derived from relative STEC by removing satellite and receiver biases [*Sardon et al.,* 1994]. This was finally converted to vertical TEC (VTEC) using a suitable mapping function with ionospheric pierce point (IPP) assumed at a height at 350 km [*Mannucci et al.,* 1993]. The elevation cut off angle of 40 degree was adopted in order to reduce multipath [*Amaechi et al.,* 2018a] as well as to reduce errors related with varying IPP due to potential ionospheric gradients [*Rama Rao et al.,* 2006]. Details about TEC processing technique can be found in *Seemala and Delay* [2010] and *Seemala and Valladares* [2011].

It is well known that 30 seconds resolution GNSS measurements can be used to monitor the temporal and spatial variability of plasma density irregularities especially, in regions void of high resolution GNSS receivers which ordinarily provide amplitude and phase scintillation data. For this purpose, the rate of change of TEC (ROT) was calculated every 30 seconds, and then converted to the unit of TECU/min. The rate of change of TEC index (ROTI) was further computed as the standard deviation of ROT over 5 minutes (i.e $ROTI = \sqrt{< ROT^2 > - < ROT >^2}$) [*Pi et al.*, 1997; *Azzouzi et al.,* 2015; *Zaourar et al.*, 2017; *Amaechi et al.,* 2018b]. It is well known that ROTI is a good proxy for scintillation index (S_4) [*Basu et al.,* 1999; *Yizengaw and Groves,* 2018]. In this work, ROTI values for all available satellites were averaged at a given epoch (5 minutes) [*Jacobsen and Dähn*, 2014; *Amaechi et al.*, 2018a] and a threshold of 0.5 TECU/ min was set as the limit for the detection of irregularities [*Ma and Maruyama*, 2006].

In selecting the storms, consideration was given to (i) their intensity (SYM-H < -100 nT), (ii) the period of occurrence (ascending and maximum phase of solar cycle 24), (iii) season of occurrence (equinoxes and solstices), (iv) simultaneous availability of GNSS data over stations located over the trough and towards the crests of the African EIA in both hemispheres. It is important to recall that the latitudinal ranges of the crests of the EIA in this sector are 4.91° to 11.70° and − 9.00° to −16.00° dip latitude [*Amaechi et al.,* 2018c].

3. Results

In this section, the description of interplanetary and magnetic conditions as well as the behavior of ionospheric irregularities over the crests and trough of the African EIA along mean longitude 37^0 is presented in Figures 2 to 8 during the storm events under consideration. All these events were CME driven except the case 1 which is a 'wake of CME' [www.spaceweather.com].

In Figure 2, changes in SYM-H, IMF *Bz*, IEFy, Diono and Ddyn as well as variations of irregularities over the crests and trough of the African EIA are presented from 21 – 26 April 2012. The SSC (vertical broken lines) started on 23 April when SYM-H (panel 1) increased sharply from 5.00 nT at 03:10 nT to 33 nT at 03:30 UT and subsequently to 45.00 nT at 04:34 UT. It however, reached a minimum value of -124.00 nT at 03:50 UT on 24 April and recovered gradually till 26 April. IMF *Bz* (second panel) went south reaching a minimum of -14.19 nT at

03:50 UT on 23 April. Convection electric field, (third panel) increased to 5.00 nT. This southward turning was nonetheless, followed by a sharp return to a northward configuration. A long duration southward turning of IMF *Bz* occurred with a minimum of -15.30 nT at 17:40 UT. Thereafter, IMF *Bz* remained south till about midnight on 23 April. Another southward turning followed by a sharp return to the northward configuration occurred at 07:00 UT with a minimum of -9.78 nT on 24 April. Convection electric field was eastward with peak amplitude of 4.01 and 5.70 mV/m during the first and second southward turning on 23 April.

The observed H (red curve, panel 4) has been superimposed on its quiet time reference level (blue curve) along with its day-by-day variation (light blue area). The quiet H clearly replicated the well-known regular pattern of the low latitude Sq for Addis Ababa. However, H increased and fluctuated at the time of SSC and was clearly below the limit of day-by-day variation with minima and oscillations opposite to its regular variations (blue curve) in the post sunset period on 23 April as well as at about 04:30 UT on 24 April. The oscillations in H were also observed in the post sunset period on 24 and 25 April. The increase in Diono was evident at the time of SSC (panel 5). Then on 23 April, Diono exhibited irregular variations with fluctuations and minima of -37.24 nT and -75.91 nT at 16:46 UT and 22:00 UT, respectively. On 24 April, the minima were -60.8n nT and -59.31 nT at 05:05 UT and 12:47 UT, respectively along with fluctuations/oscillations in the post sunset period. On 25 April, Diono fluctuations persisted with minima in the post sunset period. The amplitude of Ddyn (panel 6) was undisturbed prior to the storm day. On 23 April during the main phase, it decreased to -62.61 nT at 23:07 UT. The amplitude was -49.48 nT at 15:19 UT on 24 April; -33.96 nT at 12:33 UT on 25 April; and -7.40 nT at 17:33 UT on 26 April.

Ionospheric irregularities were observed two days before the storm (21–22 April) from 16:30 UT till midnight (panels 7- 9). Their strength was nonetheless, reduced over the trough (panel 8) and strongest over the southern crest (panel 9). On the storm day, from about 16:30 –18:00 UT, irregularities were absent (green rectangle) while they reappeared shortly over the crests at exactly 18:00 UT. Thereafter, they remained absent till midnight on 23 April and on 24–25 April. They reappeared on 26 April over the trough and northern crest. There was no data over the southern crest in the post sunset period on this day.

Figure 3 is similar to Figure 2 but is for the storm of 15 July 2012. The sharp increase in SYM-H (SSC) occurred from 8.00 nT at 18:08 UT to 51.00 nT at 18:15 UT on 14 July 2012. SYM-H reached a minimum value of -118.00 nT at 9:56 UT on 15 July and attempted a recovery to -35.00 nT at 23:35 UT on 16 July. Then, it decreased to -75.00 nT at 07:10 UT and finally returned to a quiet time variation on 18 July. IMF *Bz* fluctuated south and north at the time of SSC with corresponding fluctuations in IEFy from westward to eastward till pre-midnight on 14 July. A very long duration southward turning of IMF *Bz* however, occurred from 06:00 UT on 15 July till 14:00 UT on 16 July with minimum of -17.00 nT. During this period, IEFy was eastward with maximum amplitude of 11.23 mV/m at 07:50 UT. Another southward turning of IMF *Bz* occurred from 18:00 UT till in the early hours of 17 July with a minimum of -8.95 nT at 03:46 UT and corresponding IEFy peak of magnitude 3.60 mV/m.

The sudden increased in H and Diono occurred at about 18:14 UT on 14 July. Thereafter, H decreased gradually and was slightly below its limit of day-by-day variability at about 21:00 UT. This corresponded to a first minimum of -35.26 nT in Diono. An obvious decrease of H well below its limit of day-by-day variability occurred along with several fluctuations and day-time minima from about 03:00 – 05:00 UT and 16:00 UT on 15 July as well as 10:45 UT and 15:40 UT on 16 July; 05:50 UT and 09:15 UT on 17 July. The amplitude of H was nevertheless, reduced on 16 and 17 July. Minima in Diono were concurrently observed during the same periods. The respective amplitudes were -111.7 nT; -113.3 nT and -84.69 nT at 09:15 UT, 10:31 UT, 16.17 UT on 15 July. From 16 to 18 July, the amplitudes were -66.42 nT (10:14 UT), -51.04 nT (09:15 UT) and -34.32 nT (09:12 UT). Ddyn reached minima of -66.50 nT at 12:41 UT and -70.54 nT at 18:48 UT on 15 July as well as -46.28 nT at 13:25 UT on 16 July; -33.28 nT at 10:15 UT on 17 July; and -24.73 nT at 13:02 UT on 18 July.

Irregularities were observed over all stations on 13 July before the storm. On 14 July during the SSC, their strength was reduced over the crests while they were inhibited over the trough. They were completely absent on 15 July over all stations and remained absent on 16 July from 18:00 UT to 22:00 UT (black rectangle). From 22:00 UT to 24:00 UT they were observed over the southern crest only (red rectangle). On 17 July, only the crests experienced irregularities while on 18 July they reappeared over all stations.

Figure 4 which is the same as Figure 2 focuses on the storm of 13-14 November 2012. The SSC occurred at about 23:12 UT on 12 November while SYM-H reached a minimum of -114 nT on 14 November at about 08:00 UT (approximately one day after the arrival of the sudden shock). SYM-H recovered gradually to its quiet time variations on 17 November. IMF *Bz* went south in the post sunset period and fluctuated south and north till about early morning of 13 November. It reached a minimum of -17.71 nT at 23:30 UT. Later, IMF *Bz* went on a long southward journey from 18:00 UT on 13 November to 04:00 UT on 14 November. The minimum value reached was -17.37 nT with a corresponding IEFy peak of 7.23 mV/m at about 03:02 UT on 14 November.

On 10 November at about 08:00 UT, H was slightly below its mean quiet time variation but still within the limit of day-by-day variation. During this period, Diono and Ddyn reached respective minimum of -31.62 nT and -23.30 nT. A slight increase in H and fluctuations in Diono were observed at the time of SSC. On 13 November, an abrupt decrease in H with a corresponding minimum of -52.37 nT in Diono occurred. Prior to that, slight increases with fluctuation in Diono were observed. From about 03:00 UT on 14 November to 06:00 UT on 15 November, H decreased below the limit of day-by-day variability with fluctuations and several minima within 06:00 – 11:00 UT. Diono exhibited similar fluctuations with minima of -82.73 nT and -86.11 nT during the same period. On 15 November, H was slightly below the limit of day-by-day variability and Diono reached minimum of -39.82 nT at 07:07 UT. From 16 – 17 November, the pattern of variation of H was similar to that of its regular variation. Ddyn exhibited a first minima of -23.30 nT at 09:45 nT on 10 November whereas it was clearly disturbed with a minimum of -71.27 nT at 10:35 UT on 14 November. It reached minima of -33.26 nT at 09:42 UT and -19.09 nT at 08:08 UT on 15 November and 16 November respectively.

From 10 – 13 November and during the main phase on 14 November, no irregularities were observed over all stations. On 15 November during the recovery phase, irregularities occurred over the crests only. They were nevertheless, intense over the southern crest. On 16 November, no irregularities were observed over all stations while they reappeared on 17 November over the crests.

Figure 5 is for the St. Patrick Day storm of 17 March 2013. The SSC occurred at 06:00 UT while SYM-H reached two minima of -107 nT at about 11:56 UT and -132 nT at about 20:30 UT on 17

March. It afterwards recovered gradually to -9 nT at about 19:53 UT on 20 March but decreased again to -61 nT at 03:43 UT on 21 March. It finally returned to its undisturbed behavior by the end of the day. IMF *Bz* went south, then north and south again with minima of -15.5 nT (at 05:30 UT) and -17.73 nT (at 07:20 UT) on 17 March. From 14:35 to 21:00 UT, it went on another southward journey with minimum of -11.09 nT at 17:45 UT. During this period, IEFy was eastward with a peak of 11.90 mV/m. IMF *B*z further turned south for a short period in the pre-midnight on 20 March and early morning of 21 March. The respective minima were -7.18 mV/m and -7.22 mV/m.

On 16 March, the observed H exhibited a regular pattern similar to that of its quiet day variability. On 17 March, it decreased below the limit of day-by-day variability with fluctuations and several minima. On this day, Diono exhibited minima of -127.10 n; -100.10 nT and -70.1 nT at 10:34 UT; 12:02 UT and 16:52 UT respectively while Ddyn reached minima of -77.55 nT (13:18 UT) and -51.48 nT (20:59 UT). On 18 March, H remained slightly below the limit of day-by-day variation while Diono and Ddyn reached minima of -56.19 (08:27 UT) and -45.90 (10:43 UT) respectively. From 19-21 March, H had returned to its quiet time variation and no significant minima occurred in Diono and Ddyn.

Irregularities were observed over the crests and trough on 16 March, the day before the storm from 18:00 – 21:30 UT. During the main phase on 17 March, they were present from 17:00 – 21:30 UT, an hour earlier (Figure 5, red rectangle) over all stations. During the recovery phase on 18 – 19 March, they were absent over all stations given that ROTI values did not exceed the threshold of 0.5 TECU/min. On 19 March, no irregularities were absent over the northern crest and trough but present over the southern crest (green ellipse). On 20 March, they remained absent while they reappeared on 21 March over all stations.

Figure 6 is similar to Figure 2 but is for the storm event of 29 June 2013. At the time of SSC, SYM-H increased sharply from -12 nT at 14:40 UT to 4 nT at 14:44 UT on 27 June. On 28 it increased to 7 nT at about 04:00 UT and subsequently decreased to a minimum value of -104 nT at 06:45 UT on 29 June. The long lasting storm was characterized by a very long duration (21 hours) southward turning and eastward IEFy occurring from 02:00 UT on 28 June to 23:20 UT on 29 June. Minimum IMF *Bz* of -12.18 nT with corresponding IEFy peak of 4.73 mV/m were registered at 15:48 UT on 28 June. The H component was slightly below the limit of day-by-day variability at about 09:50 UT on 25 June. Diono reached a minimum of -38.28 nT at about the same time while Ddyn did same at about 11:22 UT (-27.63 nT). At the time of SSC on 27 June, a very weak impulse was observed in H and Diono. From about 14:00 UT on 28 June to 03:38 UT on 30 June H was clearly below the limit of day-by-day variability. Diono exhibited fluctuations and minima of -35.90 nT (04:30 UT) and -49.73 nT (16:25 UT) on 28 June as well as -66.92 nT (11:28 UT) on 29 June. The amplitude of the day-time minima was only -15.67 nT on 30 June. Ddyn exhibited minima of -24.32 nT (11:55 UT) and -32.81 nT (19:55 UT) on 28 June as well as -47.34 nT (13:15 UT) on 29 June.

On 25 June, the southern crest experienced irregularities with ROTI values slightly at the threshold of 0.5 TEU/min. On 26 – 28 June, no irregularities were observed over all stations. The peak ROTI value reach on 28 June over the southern crest was 0.455 TECU/min. Similarly, from 29 – 30 June no irregularities were observed over the crests and trough.

Figure 7 is identical to Figure 2 but deals with the storm of 19 February 2014. Magnetic conditions on 18 February were marked by a steady decrease of SYM-H from 1 nT at 13:08 UT to -47 nT by the end of the day as well as some fluctuations in IMF *B*z around 06:00 UT – 08:00 UT. IMF *Bz* went on a southward journey from about 18:30 UT till early morning of 19 February when it reached a minimum of -14.51 nT at 03:48 UT. The shock manifested in the form of a gradual increase in SYM-H from -63 nT at 02:12 UT to -51 nT at 04:17 UT when the fist CME hit the magnetopause on 19 February. This was followed by a decreased of SYM-H to -127 nT at 08:25 UT. IMF *Bz* went south reaching a minimum of -10.39 nT at about 12:00 UT. It then turned north favoring a rapid storm recovery. On 20 February during this recovery, another impulse captured as a sharp increase in SYM-H from -49 nT at 03:11 UT to -18 nT at 03:30 UT occurred. This might have been triggered when the solar filament eruption of 18 February impinged the magnetosphere. SYM-H subsequently decreased with two minima of -100 nT and -93 nT at 05:53 and 11:53 UT, respectively. During this period, three southward turning of IMF *Bz* with minima of -10.68 nT (05:07 UT), -7.72 nT (09:53 UT) and -5.19 nT (18:16 UT) occurred. On 23 February, at about 07:13 UT, following the arrival of a third CME launched on 20 February, another positive impulse of about 17 nT occurred in SYM-H while IMF *Bz* pointed northward. It nonetheless, turned southward from 14:00 – 17:00 UT with minimum IMF *Bz* of -

10.26 nT at 17:30 UT. SYM-H finally reached -50 nT at about 20:00 UT.

On 17 February at about 10:00 UT, H was below its regular variation as well as slightly outside the limit of day-by-day variability. On 18 February, it remained below this limit from about 18:00 – 24:00 UT. On 19 – 20 February, H was still below this limit with oscillation and minima around noon. On 21 – 22 February, it remained slightly below the regular variation while on 23 February it increased suddenly at the arrival of the shock at 07:13 UT. H was thereafter, below the limit of day-by-day variation with a minimum registered at about 18:51 UT. Diono registered its first minimum of -35.47 nT at 11:22 UT on 17 February. On 19 and 20 February, several oscillations in Diono with minima of -52.42 nT (09:55 UT) and -98.74 nT (08:16 UT) were observed. On 21 February the minimum was -35.53 nT (10:55 UT) while it was -44.54 nT (09:51 UT) and -61.67 nT (18:51 UT) on 22 and 23 February respectively. Oscillations in Ddyn with weak amplitude were observed from 18 – 20 February. The amplitude of Ddyn was pronounced on 21 February while it reduced on 22 February. On 23 February, the pattern of oscillations was a little different from those of the previous days. The first minimum in Ddyn occurred at 14:17 (-28.58 nT) on 17 February. Other minima of -19.33 nT were recorded at 12:01 UT on 19 February; -64.51 nT at 10:00 UT on 20 February; -28.12 nT at 13:39 UT on 21 February; -33.06 nT at 13:09 UT on 22 February; and -50.54 nT at 20:28 UT on 23 February.

Ionospheric irregularities were observed two days prior to the main phase of the storm (17 and 18 February) over all stations. Their strength was pronounced over the northern crest. During the main phase on 19 February, irregularities were absent while they reappeared on 20 February over all stations. On 21 - 22 February they were absent while on 23 February they reappeared over all stations.

The St. Patrick's Day storm of 17 March 2015 has received considerable attention mainly because it is the most intense storm of solar cycle 24 so far. Interplanetary and magnetic conditions during this event have been described in several literatures [e.g. *Borries et al.,* 2016; *Nayak et al.,* 2016; *Nava et al., 2016; Rajesh et al., 2017*; *Amaechi et al.,* 2018a,b]. Emphasis will thus, be placed on key features of the interplanetary response only. From Figure 8, the SSC started on 17 March with an abrupt increase in SYM-H from 13 nT to 67 nT within 04:35 – 04:50 UT. SYM-H then decreased and reached minima of -101 nT and -228 nT at 09:34 UT and

22:57 UT respectively. It thereafter, recovered steadily to its quiet time value towards the end of 21 March. IMF *Bz* went south twice within 06:00 – 09:00 UT with minima of -21.06 nT and -20.83 nT at about 06:00 UT and 07:30 UT respectively, on17 March and corresponding peak eastward IEFy of 10.9 nT and 11.96 nT. It latter went on a long duration southward journey from noon to midnight with minimum of -26.57 nT at 12:40 UT.

H decreased below its limit of day-by-day variability with several minima at 09:50 UT, 16:51 UT and 19:40 UT on 17 March. On 18 and 19 March H was opposite to its regular variation from 09:00 – 15:00 UT. Diono exhibited several oscillations with minima of -131 nT (09:58 UT); -166.20 nT (17:00 UT) and -114.30 nT (19:00 UT) on 17 March as well as -118.40 nT (10:40 UT) on 18 March; -68.67 nT (12:11 UT) on 19 March and -39.15 nT (10:14 nT) on 20 March. Ddyn exhibited similar minima at 17:50 UT (-127.30 nT) on 17 March; 12:00 UT (-100.10 nT) on 18 March; 13:24 UT (-75.35 nT) on 19 March and 11:45 UT (-42.22 nT) on 20 March.

On 16 March, the day before the storm, irregularities were observed while during the main phase on 17 March, they were absent over all the stations. During the recovery phase, they remained absent on 18 and 19 March but reappeared on 20 and 21 March over all stations. They were stronger over the southern crest before the storm and were of short duration during the recovery phase on 20 March.

Figure 9 presents variations of the PPEF derived from the PPEFM during the main phases of the storms. The PPEF + Quiet EEF (red line) has been superposed to the Quiet EEF (dark line). Quiet EEF was obtained by taken the average of the 5 quietest days shown in Table 2. It can be observed that on 23 April 2013, there was no obvious PPEF effect in the early hours of the morning. However, in the post sunset, the PRE was increased slightly at the time when IMF *Bz* was south (Figure 9a). On 15 July 2012, PPEF + Quiet EEF was clearly higher than Quiet EEF indicating the present eastward PPEF (Figure 9b). On 13 November 2012, PPEF reduced the PRE slightly in the post sunset period (Figure 9c) while on 17 March 2013, two eastward PPEF can be observed in the morning while another one enhanced the PRE in the post sunset period (Figure 9d). On 28 June 2013, the effect of PPEF could be seen as an increase in the early morning period (Figure 9e) while on 19 February 2014, it was appeared in the noon and post sunset periods. The post sunset PRE was consequently reduced (Figure 9f). Finally, on 17 March

2015, the effect of the two PPEFs was obvious during the noon period while there was a data gap in the post sunset period (Figure 9g). Characteristics features of the irregularities variations during the storm events analyzed are summarized in Table 3 and discussed in the next section.

4. Discussion

It is well known that during storm, PPEF and DDEF can affect the regular eastward electric field (ie, upward $E \times B$) hence, the formation of ionospheric irregularities [*Abdu et al.,* 2009, 2018]**.** When IMF *Bz* turns south and convection electric field (IEFy) increases, PPEF whose signature is the DP2 signal can penetrate into the low-latitude ionosphere [*Kikuchi and Akari,* 1979]. The disturbed electric field can be captured in the form of a perturbation in the H component and short-term oscillations of Diono [*Nava et al.,* 2016] especially during the beginning of a storm [*Amory-Mazaudier et al.,* 2017]. However, the time of occurrence of PPEF is crucial in influencing the pattern of irregularities. For example, eastward PPEFs that occurred in the morning period (06:50 LT on 23 April 2012; 15:00 LT on 17 March 2013; 15:00 LT on 19 February 2014; and 09:00 - 12:00 LT on 17 March 2015) could not last long enough to influence the pattern irregularities in the post sunset. Also, the presence of westward PPEF in the nighttime (local pre-midnight of 14 July 2012; 02:30 LT on 12 November 2012; and 18:00 - 23:30 on 17 March 2015) acted to suppress the PRE and create conditions unfavorable for the development of irregularities. *Chakraborty et al.* [2015] had previously observed that eastward IEF Ey was opposite to zonal electric field thus, failed to enhance the upward $\boldsymbol{E}\times\boldsymbol{B}$ plasma drift in the local night-time hour of the Indian sector on 14 July 2012.

On the other hand, during the southward turnings of IMF *Bz* that took place at about 20:40 LT on 23 April, 17:35 – 24:00 LT on 17 March 2013 and 21:00 LT on 20 February 2014, eastward PPEFs occurred in the post sunset period and enhanced the upward $\boldsymbol{E} \times \boldsymbol{B}$ drift. This in turn triggered short duration irregularities over the crests and weak ones over the trough on 23 April (Figure 2) but also an hour earlier on 17 March (Figure 5, red box) as well as in the pre-midnight period of 20 February 2014 (Figure 7). The result of 23 April is particularly interesting giving that irregularities were earlier inhibited by westward electric field (Figure 2, Green box). In line with our observations on 17 March, *Kalita et al.* [2016] found that short duration irregularities were triggered when IMF *Bz* turned south in the sunset period over 100^{o} E longitude. In the same vein, *Kassa and Damtie* [2017] reported that irregularities were triggered over Bahir Dah (11^{o}N, 38^{o}E), Ethiopia by an enhanced drift which had favored the post sunset lifting of the F-layer [*Joshi et al.,* 2015] to altitude where irregularities were generated by the R-T instability mechanism [*Kelley*, 1989; *Yizengaw and Groves*, 2018].

Conversely, DDEF are more active during the recovery phase of geomagnetic storm. The decay in H several hours after the beginning of the disturbance is the signature of Ddyn current system [*Azzouzi et al*., 2015] related to westward DDEF [*Le Huy and Amory-Mazaudier*, 2008]. Westward DDEF are driven by increased heating of the thermosphere at high latitude ensuing from the energy input over this region during storms [*Danilov and Lastovicka,* 2001] and their occurring in the post sunset period can inhibit the development of irregularities [*Adbu et al.,* 1995]. The minima in Ddyn in the post sunset is evidence of the presence of DDEF which must have been responsible for the inhibition of irregularities over the crests and trough of the EIA on 24-25 April 2012, 15-16 July 2012, 18 March 2013, 19 February and 21-22 February as well as 17 – 19 March 2015 (Table 3). *Kassa and Damtie* [2017] had similarly reported a sharp drop in irregularities level on 19 February 2014 and a prolonged suppression thereafter, over Bahir Dah (11^{o}N, 38^{o}E), Ethiopia**.** It is important to note that the duration of irregularities inhibition lasted longer during the super storm of March 2015 (3 days) than the other storms (1-2 days). Using spectral analysis, *Nava et al.* [2016] showed that DDEF lasted for about 6 days during this super storm over Africa.

Additionally, westward DDEF can occur when the southward turning of IMF *Bz* is followed by a rapid return to northward and there is rapid decrease in convection during the main phase [*Kikuchi et al.*, 2000]. Stressing further, *Kikuchi et al.* [2003] postulated that when R2-FACs build up following the rapid decrease in R1-FACs, due to the northward turning of the IMF and concomitant decreased in convection, electric field at the equatorial region reverse from eastward to westward under the so-called dominant shielding electric field [*Kelley et al.,* 1979]. Recently, *Huang* [2018] confirmed that it takes about 4.7 hours after the onset of a storm for the effect of disturbance dynamo to reach the equatorial region. It is thus, inferred that westward disturbed electric field were responsible for the short duration (20:00 – 21:00 LT) inhibition of irregularities on 23 April (Figure 2, green box).

The occurrences of irregularities near the trough cannot be explained by electric fields only. The PRE occurs in the post sunset when solar photoionisation decreases rapidly, consequently there are large density gradients thus irregularities develop thanks to the R-T instabilities. Background density is thus, a crucial factor to reckon with in the formation of irregularities. The small background density at 06:20 LT on 23 April as well as at 02:12 LT in winter (12 November 2012) might have provided unfavorable condition for the formation of irregularities. Furthermore, irregularities are less frequent in solstices than in equinoxes due to the fact that the eastward electric field is smaller at solstices than at equinoxes and as a consequence solstice conditions are unfavorable for bubbles formation. This also explains the absence of irregularities during the storms of November 2012 and June 2013.

Previous work by *Amaechi et al.,* [2018ab] had studied variations of irregularities near the magnetic equator. However, such studies were limited to 4 storms which occurred in the same year (2015). The present work further generalized the analysis with 7 new storms occurring during 4 different years (2012, 2013, 2014, 2015), as well as seasons (Equinox, Summer, Winter). The new finding is that there are common features for irregularities response to all the storms over the trough of the African EIA, eventhough these storms appear to be different. In addition, irregularities inhibition is found to last longer during super storm than intense storms.

Irregularities occurrences over the EIA crests is quite complex. The triggering of strong irregularities over the crests (ROTI $\geq$ 1) and weak ones over the trough (ROTI ~ 0.5) on 23 April 2012 and 20 February 2014 is consistent with EPBs being generated at the magnetic equator by the R-T instability, their movement higher up, and subsequent extension along the magnetic field lines before they eventually reach the crests [*Ossakow,* 1981; *Groves et al.,* 1997]. Nevertheless, the fact that irregularities were inhibited over the trough and present over the crests on 16 - 17 July, 15 November 2012 and 19 March 2013 suggested that they did not originate from the magnetic equator but might have been generated locally or might have come from the mid-latitude. It is known that forces from below mainly, propagating atmospheric waves and the related travelling ionospheric disturbances (TIDs) can initiate perturbation which might lead to the development of irregularities [*Yizengaw and Groves,* 2018]. Medium-scale travelling ionospheric disturbances (MSTIDs) originating from mid-latitude can be responsible for irregularities over the crests of the anomaly [*Matthew et al.,* 1991]. On the other hand, changes in neutral wind during the recovery phase can also affect the R-T instability. *Maruyama and Matuura*, [1984] showed that various forms of plasma transport by meridional wind from one hemisphere to another can affect conductivity thus, the RT instability growth rate. Another contributing factor could have been the asymmetry of the EIA crests in Africa. It has been shown that strong asymmetry exist in the latitudinal position and magnitude of the crests of the EIA in both hemispheres with the southern crest forming farther from the magnetic equator and having greater peaks in the post sunset period [*Amaechi et al.,* 2018c]. However, the influence of perturbations from the lower atmosphere and the related gravity waves on the pattern of irregularities as well as the contribution of the asymmetry of the EIA crests over Africa during the recovery phase of intense storms still requires further investigations.

First result for the assessment of the capability of the PPEFM over the African longitude revealed that the model is capable of reproducing accurately eastward and westward PPEF as well as the corresponding effect on the PRE hence, on the triggering and inhibition of irregularities during all the storms under consideration. Nayak et al [2016] had used the same model to show how eastward PPEF/ westward DDEF reduced /enhanced the PRE thus on generating/inhibiting irregularities in the Indian/ Taiwanese sectors during the storm of 17 March 2015. Validating the PPEFM in the present study further reinforces the role of modeling in increasing our understanding of storm time electric field effect on irregularities over the low-latitude African sector**.**

5. Conclusions

The behavior of ionospheric irregularities over the African EIA has been studied during intense geomagnetic storms of the ascending phase of solar cycle 24. Emphasis was placed on the simultaneous response over the crests and on the capability of PPEFM to predict PPEFs along longitude 37^{o}E. It was found that:

1. The timing of occurrence of PPEF was a crucial factor affecting the behavior of irregularities. As such, despite the presence of westward DDEF that had suppressed irregularities for over one hour on 23 April 2012, an eastward PPEF which occurred at about 21:00 LT triggered them over the crests of the African EIA but for a short period.

2. The existence of a long duration eastward PPEF triggered irregularities one hour earlier on 17 March 2013 over the trough and crests. However, westward DDEF that developed thereafter inhibited them for the rest of the night. Another eastward PPEF which occurred at about 21:00 LT triggered irregularities on 20 February 2014.

3. The PPEFM reproduced fairly well the PPEF during the main phase of the events. It was thus, found to be accurate at least based on our observations.

4. No irregularities were observed during the storms of November 2012 and June 2013 while they were suppressed during the recovery phases of the storm of April 2012; July 2012; March 2013; February 2014 and March 2015 by westward disturbed electric field. In addition, the H component was always opposed to its regular variations several hours after the beginning of the disturbance in agreement with existing theories of Ddyn (Blanc and Richmond, 1980). However, the amplitude and duration of the magnetic disturbance Ddyn varied from one storm to another.

5. Irregularities were always inhibited over the trough but the inhibition lasted longer during the super storm of March 2015. Over the crests, there was an asymmetry in their strength which was linked to the asymmetry in magnitude and position of the EIA crests over Africa.

6. During the recovery phase, significant differences in irregularities existed over crests. The southern crests experienced irregularities on 16 July 2012 and 19 March 2013 while the northern crest and trough did not. In addition, both crests experienced irregularities on 17 July 2012 and 15 November 2012.

The behavior of irregularities over the African EIA crests suggests the existence of non equatorial processes capable of generating them locally and/or their association with MSTID originating from mid-latitude. Unfortunately the African longitude is void of observational tools such as incoherent scatter radar (ISR) that could have given us more insight into the variations of electric field as well as the contribution of perturbation originating from the lower atmosphere during these events.

Acknowledgements

The authors wish to thank the ISGI (htpp://isgi.unistra.fr) for the SYM-H data; the ACE SWEPAM teams (http://www.srl.caltech.edu/ACE/ASC/level2/) for providing the IMF *Bz* and Vx data; the INTERMAGNET team (www.intermagnet.com) for the magnetometer data and UNAVCO (htpp://www.unavco.org/data/data.html) for the GNSS observables. The Prompt penetration equatorial electric field model data were obtained from http://www.geomag.org/models/PPEFM/ RealtimeEF.html. The CME catalog is generated and maintained at the CDAW Data Center by NASA and The Catholic University of America in cooperation with the Naval Research Laboratory. SOHO is a project of international cooperation between ESA and NASA.

The authors thank two anonymous reviewers for their useful comments that significantly improved the quality of this manuscript.

References

Aarons, J., M. Mendillo, R. Yantosca, and E. Kudeki (1996), GPS phase fluctuations in the equatorial region during the MISETA 1994 campaign, *J. Geophys. Res*., 101(A12), 26,851-26,862.

Aarons, J. (1982), Global Morphology of Ionospheric Scintillations, Proceeding of the IEEE. 70(4), 360-378.

Abdu, M. A., P. A. B. Nogueira, A. M. Santos, J. R. de Souza, I. S. Batista, and J. H. A. Sobral (2018), Impact of disturbance electric fields in the evening on prereversal vertical drift and spread F developments in the equatorial ionosphere, *Ann. Geophys*., 36, 609–620.

Abdu, M. A. (2012), Equatorial spread F/plasma bubble irregularities under storm time disturbance electric fields, *J. Atmos. Terr. Phys*., 75–76, 44–56.

Abdu, M. A., E. A. Kherani, I. S. Batista, and J. H. A. Sobral (2009), Equatorial evening prereversal vertical drift and spread F suppression by disturbance penetration electric fields, *Geophys. Res. Lett*., 36, L19103.

Abdu, M. A., I. S. Batista, G.O. Walker, J. H. A. Sobral, N. B. Trivedi, and E. R. de Paula (1995), Equatorial ionospheric electric fields during magnetospheric disturbances: Local time/longitudinal structure and spread F: A case study from GUARA/EITS campaigns, *Geophys.Res. Lett*., 57(10), 1065–1083.

Amaechi, P. O., E. O. Oyeyemi, and A. O. Akala (2018a), Geomagnetic storm effects on the occurrences of ionospheric irregularities over the African equatorial/low-latitude region, *Adv. Space Res*., 61, 2070–2090.

Amaechi, P. O., E. O. Oyeyemi, and A. O. Akala (2018b), The response of African equatorial/ low-latitude ionosphere to 2015 St. Patrick's Day geomagnetic storm, *Space Weather*, 16, 601–618.

Amaechi, P. O., E. O. Oyeyemi, and A. O. Akala (2018c), Variability of the African equatorial ionization anomaly (EIA) crests during the year 2013, *Can. J. Phys.* 97(2), 155-165.

Amory-Mazaudier, C., O. S. Bolaji, and V. Doumbia (2017), On the historical origins of the CEJ, DP2, and Ddyn current systems and their roles in the predictions of ionospheric responses to geomagnetic storms at equatorial latitudes, *J. Geophys. Res.*, 122, 7827–7833.

Appleton, E.V. (1946), Two anomalies in the ionosphere, *Nature.* 157(3995), 691.

Azzouzi, I., Y. Migoya-Orue, C. Amory-Mazaudier, R. Fleury, S. M. Radicella, and A. Touzani (2015), Signature of solar event at middle and low latitudes in the European- African sector, during geomagnetic storms, October 2013, *Adv. Space Res.*, 56(9), 2040– 2055.

Basu, S., K M. Groves, J .M. Quinn, and P. Doherty (1999), A comparison of TEC fluctuations and scintillations at Ascension Island, *J Atmos. Terr. Phys*., 61, 1219–1226.

Blanc, M., and A. D. Richmond (1980), The Ionospheric disturbance dynamo. *J. Geophys. Res.*, 85(A4), 1669–1686.

Blewitt, G. (1990), An automatic editing algorithm for GPS data, *Geophys. Res. Lett.*, 17(2), 199–202.

Borries, C., A. M. Mahrous, N. M., Ellahouny, and R. Badeke (2016), Multiple ionospheric perturbations during the Saint Patrick's Day storm 2015 in the European-African sector, *J. Geophys. Res.*, 121, 11,333–11,345.

Carter, B. A., et al. (2014), Geomagnetic control of equatorial plasma bubble activity modeled by the TIEGCM with *Kp*, *Geophys. Res. Lett.*, *41*, 5331–5339.

Chakraborty, M., S. Kumar, A. Guha, B. K. De (2015), Effects of geomagnetic storm on low latitude ionospheric total electron content: A case study from Indian sector, J. Earth Syst. Sci., 124(5), 1115-1126.

Chakrabarty, D., R. Sekar, R. Narayanan, C. V. Devasia, and B. M. Pathan (2005), Evidence for the interplanetary electric field effect on the OI 630.0 nm airglow over low latitude, *J. Geophys. Res.*, 110, A11301.

Chapman, S. (1919), An outline of the theory of magnetic storms, *Proc. R. Soc. London, Ser.*, A, 95, 61.

Chapman, S., and V. C. A. Ferraro (1931), A new theory of magnetic storms, *Terr. Magn. Atmos. Elec.*, 36, 77- 97.

Cole, K. D. (1966), Magnetic storms and associated phenomena, *Space Sci. Rev.*, 5, 699–770.

Conker, R. S., M. B. El-Arini, C. J. Hegarty, and T. Hsiao (2003), Modeling the effects of ionospheric scintillation on GPS/Satellite-Based Augmentation System availability, *Radio Sci.*, 38(1), 1-1.

Danilov, A.D., and J. Lastovicka (2001), Effects of geomagnetic storms on the ionosphere and atmosphere, *Int. J. Geom. Aero*, 2, 209–224.

Datta-Barua, S., Y. Su, K. Deshpande, D. Miladinovich, G. S. Bust, D. Hampton, and G. Crowley (2015), First light from a kilometer-baseline Scintillation Auroral GPS Array, *Geophys. Res. Lett.*, 42(10), 3639-3646.

Eccles, J. V. (2004), Assimilation of global-scale and mesoscale electric fields from low-latitude satellites, *Radio Sci.*, *39*, RS1S09.

Estey, L. H., and C. M. Meertens (1999), TEQC: The multi-purpose toolkit for GPS/ GLONASS data, *GPS Solutions*, 3(1), 42–49.

Farley, D. T., B. B. Balsey, R. F. Woodman, and J. P. McClure (1970), Equatorial spread F: Implications of VHF radar observations, *J. Geophys. Res.*, 75(34), 7199-7216.

Fathy, I., C. Amory-Mazaudier, A. Fathy, A. M. Mahrous, K. Yumoto, and E. Ghamry (2014), Ionospheric disturbance dynamo associated to a coronal hole: Case study of 5–10 April 2010, *J. Geophys. Res.*, 119, 4120–4133.

Fejer, B. G., M. Blanc, and A.D. Richmond (2016), Post-storm middle and low-latitude ionospheric electric fields effects. Space Sci. Rev., 206(1-4), 407-429.

Fejer, B.J., L. Scherliess, and E. R. de Paula (1999), Effects of the vertical plasma drift velocity on the generation and evolution of equatorial spread F, *J. Geophys. Res.*, 104 (A9), 19859 -19,869.

Fejer,B.G., and L. Scherliess (1997), Empirical models of storm time equatorial zonal electric fields, *J. Geophys. Res*., 102, AII, 24,047-24,056.

Fuller-Rowell, T. J., M. V. Codrescu, R. G. Roble, and A. D. Richmond (1997), How does the thermosphere and ionosphere react to a geomagnetic storm?, *Magnetic storms*, *98*, 203-225.

Groves, K.M., S. Basu, E. J. Weber, M. Smithan, H. Kuenzler, C. E. Valladares, R. Sheehan, E. Mackenzie, J. A. Secan, P. Ning, W. J. McNeill, D. W. Moonan, and M. J. Kendra (1997), Equatorial scintillation and system support, *Radio Sci*., 32, 2047–2064.

Hairston, M., W. R. Coley, and R. Stoneback (2016), Responses in the polar and equatorial ionosphere to the March 2015 St. Patrick Day storm, *J. Geophys. Res*., 121, 11,213–11,234.

Haerendel, G. (1973), *Theory of equatorial spread F*, preprint, Max Plank Inst. for Extra terr. Phys., Munchen, Germany.

Hansen, A., J. Blanch, and T. Walter (2000), Ionospheric correction analysis for WAAS quiet and stormy (pp. 634–642). ION GPS, Salt Lake City, Utah, September 19-22.

Heelis, R. A. (2004), Electrodynamics in the low and middle latitude ionosphere: A Tutorial, *J. Atmos. Solar-Terr. Phys*., 66(10), 825-838.

Huang, C-S. (2018), Effects of Geomagnetic Storms on the Postsunset Vertical Plasma Drift in the Equatorial Ionosphere, *J. Geophys. Res*., 123, 5.

Jacobsen, K.S., and M. Dähnn (2014), Statistics of ionospheric disturbances and their correlation with GNSS positioning errors at high latitudes, *J. Space Weather Space Clim.* 4, A27.

Joshi, L. M., S. Balwada, T. K. Pant, and S. G. Sumod (2015). Investigation on F layer height rise and equatorial spread F onset time: Signature of standing large-scale wave, *Space Weather*, 13(4), 211-219.

Kakad, B., C. K. Nayak, and A. Bhattacharyya (2012), Power spectral characteristics of ESF irregularities during magnetically quiet and disturbed days, *J. Atmos. Sol. Terr. Phys*., 81, 41-42.

Kalita, B. R., et al. (2016), Conjugate hemisphere ionospheric response to the St. Patrick's Day storms of 2013 and 2015 in the 100°E longitude sector, *J. Geophys. Res.*, 121, 11.

Kamide, Y., and N. Fukushima (1972), Positive geomagnetic bays in evening high latitudes and their possible connection with partial ring current, *Rep. Ionos. Space Res. Jap.*, 26, 79-

101.

Kassa, T., B. Damtie (2017), Ionospheric irregularities over Bahir Dar, Ethiopia during selected geomagnetic storms. *Adv. Space Res.*, 60(1), 121–129.

Kelley, M. C. (1989), *Ionospheric Radio.* Peter Peregrinus Ltd. London.

Kelley, M. C., B. G. Fejer, and C. A. Gonzales (1979), An explanation for anomalous equatorial ionospheric electric fields associated with a northward turning of the interplanetary magnetic field, *Geophys. Res. Lett*., 6, 301–304.

Kikuchi, T., K. K. Hashimoto, and K. Nozaki (2008), Penetration of magnetospheric electric fields to the equator during a geomagnetic storm, *J. Geophys. Res*., 113(A6).

Kikuchi, T., K. Hashimoto, T.-I. Kitamura, H. Tachihara, and B. Fejer (2003), Equatorial counter electrojets during substorms, *J. Geophys. Res*., 108(A11), 1406.

Kikuchi, T., H. Lühr, K. Schlegel, H. Tachihara, M. Shinohara, and T.I-. Kitamura (2000), Penetration of auroral electric fields to the equator during a substorm, *J. Geophys. Res.,* 105, 23,251–23,261.

Kikuchi, T., and T. Araki (1979), Transient response of uniform ionosphere and preliminary reverse impulse of geomagnetic storm sudden commencement, *J. Atmos. Terr. Phys.*, 41, 917–925.

Kintner, P.M., B. M. Ledvina, and E. R. de Paula (2007), GPS and ionospheric scintillations, *Space Weather*, 5, S09003.

Kudeki, E., A. Akgiray, M. Milla, J. L. Chau, and D. L. Hysell (2007), Equatorial spread-F initiation: Post-sunset vortex, thermospheric winds, gravity waves, *J. Atmos. Solar-Terr. Phys*., 69(17-18), 2416-2427.

Kuznetsov, B. M., and O.A. Troshichev (1977), On the nature of polar cap magnetic activity during undisturbed periods. *Planet. Space Sci.*, *25*(1), 15-21.

Le Huy, M., and C. Amory-Mazaudier (2008), Planetary magnetic signature of the storm wind disturbance dynamo currents: Ddyn, *J. Geophys. Res.*, 113, A02312.

Le-Huy, M., and C. Amory-Mazaudier (2005), Magnetic signature of the ionospheric disturbance dynamo at equatorial latitudes, “Ddyn”, *J. Geophys. Res*., 10, A10301.

Liu, J., L. Liu, T. Nakamura, B. Zhao, B. Ning, and A. Yoshikawa (2014), A case study of ionospheric storm effects during long-lasting southward IMF Bz-driven geomagnetic storm, *J. Geophys. Res.* 119, 7716–7731.

Ma, G., and T.Maruyama (2006), A super bubble detected by dense GPS network at East Asian longitudes, *Geophys. Res. Lett*., 33, L21103.

Mannucci, A. J., B. D. Wilson, and C. D. Edwards (1993), A new method for monitoring the Earth's ionosphere total electron content using the GPS global network. Proceedings of ION GPS-93, Institute of Navigation (pp. 1323–1332).

Manoj, C., and S. Maus (2012), A real-time forecast service for the ionospheric equatorial zonal electric field, *Space Weather*, 10(9), 1-9.

Manoj, C. S. M., S. Mus, H. Lühr, and P. Alken (2008). Penetration characteristics of the interplanetary electric field to the day-time equatorial ionosphere, *J. Geophys. Res. Atm.*, 113 (A12).

Maruyama, T., and N. Matuura (1984), Longitudinal variability of annual changes in activity of equatorial spread F and plasma bubbles, *J. Geophys. Res*. 39, 10903–10912.

Mathew, B., B.M. Pathan, K.N. Iyer, D.R.K. Rao (1991), Comparative study of scintillations at the magnetic equator and at the crest region of the equatorial anomaly in Indian zone. *Proceedings of the Indian Academy of Sciences-Earth and Planetary Sciences*, *100*(4), 331-340.

Mayaud, P. N. (1965), Analyse morphologique de la variabilité jour-à-jour de la variation journalière régulière SR du champ magnétique terrestre, I- le système de courants Cp (régions polaires et subpolaires), *Ann. Geophys.*, 21, 369-401.

Mungufeni, P., J. B. Habarulema, and E. Jurua (2016), Trends of ionospheric irregularities over African low latitude region during quiet time geomagnetic conditions, *J. Atmos. Sol. Terr. Phys*., 138–139, 261–267.

Nava, B., J. Rodríguez-Zuluaga, K. Alazo-Cuartas, A. Kashcheyev, Y. Migoya-Orué, S. M. Radicella, C. Amory-Mazaudier, and R. Fleury (2016), Middle and low latitude ionosphere response to 2015 St. Patrick's Day geomagnetic storm, *J. Geophys. Res.*, 121, 3421–3438.

Nayak, C., L.-C. Tsai, S.-Y. Su, I. Galkin, R. Caton, and K. Groves (2016). Suppression of ionospheric scintillation during St. Patrick's 24 Day geomagnetic super storm as observed over the anomaly crest region station Pingtung, Taiwan: A case study, *Adv. Space Res.*, 60, 396-405.

Nishida, A. (1968), Geomagnetic DP2 fluctuations and associated magnetospheric Phenomena,

J. Geophys.Res., 73, 1795–1803.
Nishida, A., N. Iwasaki, and T. Nagata (1966), The origin of fluctuation in the equatorial electrojet: a new type of geomagnetic variation, *Ann. Geophys*., 22, 478.
Ngwira, C. M., J. Klenzing, J. Olwendo, F. M. D'ujanga, R. Stoneback, and P. Baki (2013), A study of intense ionospheric scintillation observed during a quiet day in the East African low-latitude region, *Radio Sci*., 48, 396–405.
Olwendo, O. J., Y. Yamazak, P. Cilliers, P. Baki, C. M. Ngwira, and C. Mito (2015), A study on the response of the Equatorial Ionization Anomaly over the East Africa sector during the geomagnetic storm of November 13, 2012. *Adv. Space Res.*, 55(12), 2863-2872.
Ossakow, S. L. (1981), Spread-F theories–A review, *J. Atmos. Solar-Terr. Phys*., 43, 437-443.
Ott, E. (1978), Theory of Rayleigh-Taylor bubbles in the equatorial ionosphere, *J. Geophys. Res*., 83(A5), 2066-2070.
Paznukhov, V. V., C. S. Carrano, P. H. Doherty, K. M. Groves, R. G. Caton, C. E. Valladares, G. K. Seemala, C. T. Bridgwood, J. Adeniyi, L. L. N. Amaeshi, B. Damtie, F. D'Ujanga Mutonyi, J. O. H. Ndeda, P. Baki, O. K. Obrou, B. Okere, G. M. Tsidu (2012), Equatorial plasma bubbles and L-band scintillations in Africa during solar minimum, *Ann. Geophys.,* 30, 675–682.
Perkins, F.W. (1975), Ionospheric irregularities, *Rev. Geophys. Space Phys*., 13(3), 884.
Pi, X., A. J. Manucci, U. J. Lindqwister, and C. M. Ho (1997), Monitoring of global ionospheric irregularities using the worldwide GPS network, *Geophys. Res. Lett.*, 24, 2283–2286.
Rama Rao, P.V. S., K. Niranjan, D.S.V.V.D. Prasad, S. K. Gopi, and G. Uma (2006), On the validity of the ionospheric pierce point (IPP) altitude of 350 km in the Indian equatorial and low-latitude sector, *Ann. Geophys*., 24, 2159–2168.
Rostoker, G. (1969), Classification of Polar magnetic disturbances, *J. Geophys. Res.*, 74, 21, 5161.
Rostoker, G. A. (1967), Determining factor in the form of the equivalent current system for geomagnetic bays, Earths Planetary Sci. Letters, 2, 119.
Sabaka, T. J., N. Olsen, and M. E. Purucker (2004), Extending comprehensive models of the Earth magnetic field with Oersted and Champ data, *Geophys. J. Int*., 159, 521–547.
Sardon, E., A. Rius, and N. Zarraoa (1994), Estimation of the transmitter and receiver

differential biases and the ionospheric total electron content from GPS observations, *Radio Sci*., 29(3), 577–586.

Scherliess, L., and B. G. Fejer (1997), Storm time dependence of equatorial disturbance dynamo zonal electric fields, *J. Geophys. Res.*, 102(A11), 24,037–24,046.

Semala, G.K., and C. E. Valladares (2011), Statistics of TEC depletions observed over the South American continent for the year 2008, *Radio. Sci.*, 46, RS5019.

Seemala, G., and S. B. Delay (2010), GNSS TEC data processing, 2nd Workshop on Satellite Navigation Science and Technology for Africa, Trieste, 6-24 April 2010.

Stauning, P. (2012), The Polar Cap PC Indices: Relations to Solar Wind and Global Disturbances, Exploring the Solar Wind, Dr. Marian Lazar (Ed.), ISBN: 978-953-51-0339-4.

Sultan, P. J. (1996), Linear theory and modeling of the Rayleigh-Taylor instability leading to the occurrence of equatorial spread F, *J. Geophys. Res.,* 101(A12), 26,875-26,891.

Sunda, S., R. Sridharan, B. M. Vyas, P. V. Khekale, K. S. Parikh, A. S. Ganeshan, C. R. Sudhir, S. V. Satish, and M. S. Bagiya (2015), Satellite-based augmentation systems: A novel and cost-effective tool for ionospheric and space weather studies. *Space Weather*, 13(1), 6-15.

Svalgaard, L. (1968), Sector structure of the interplanetary magnetic field and daily variation of the geomagnetic field at high-latitudes. Danish. *Meteor. Inst. Geophys. Paper,* R-6.

Thampi, S. V., P. R. Shreedevi, R.K.Choudhary,T. K. Pant, D. Chakrabarty, S. Sunda, S. Mukherjee, and A. Bhardwaj (2016), Direct observational evidence for disturbance dynamo on the day-time low-latitude ionosphere: A case study based on the 28 June 2013 space weather event, J. Geophys. Res., 121, 10,064–10,074.

Troschichev, O., and A. Janzhura (2012), Space Weather Monitoring by Ground-Based Means: PC Index. Springer, Chichester, UK.

Tsunoda, R. T., S. V. Thampi, T. T. Nguyen, and M. Yamamoto (2013), On validating the relationship of ionogram signatures to large-scale wave structure, *J. Atmos. Solar-Terr. Phys.*, 103, 30-35.

Tsunoda, R. T. (2010), On equatorial spread F: establishing a seeding hypothesis, *J. Geophys.,* 115, A12303.

Vasyliunas, V. M. (1970), Mathematical models of magnetospheric convection and its coupling to the ionosphere. In *Particles and Fields in the Magnetosphere* (pp. 60-71). Springer, Dordrecht.

Wanliss, J.A., and K. M. Showalter (2006), High-resolution global storm index: Dst versus SYM-H, *J. Geophys. Res.*, 111, A02202.

Yizengaw, E., and K. M, Groves (2018), Longitudinal and Seasonal Variability of Equatorial Ionospheric Irregularities and Electrodynamics, *Space Weather*, 16(8), 946-968.

Yizengaw, E., J. Retterer, E. E. Pacheco, P. Roddy, K. Groves, R. Caton, and P. Baki (2013a), Post-midnight Bubbles and Scintillations in the Quiet-Time June Solstice, *Geophys. Res. Lett.*, 40, 5592-5597.

Yizengaw, E., P. Doherty, and T. Fuller-Rowell (2013b), Is Space Weather Different Over Africa, and If so, Why? AGU Chapman Conference Report, *Space Weather*, 398-391.

Yue, X., W. S. Schreiner, Y. H. Kuo, and J. Lei (2015), Ionosphere equatorial ionization anomaly observed by GPS radio occultation during 2006–2014, *J. Atmos. Solar-Terr. Phys.*, 129, 30-40.

Zaourar, N., C. Amory-Mazaudier, and R. Fleury (2017), Hemispheric asymmetries in the ionosphere response observed during the high-speed solar wind streams of the 24-28 August 2010, *Adv. Space Res.*, 59(9), 2229-2247.

Tables caption

Table 1: Coordinates of the GPS and magnetometer stations.

Table 2: Magnetic quietest days during each storm. These are five international quietest days provided by GFZ, Helmholtz Postdam Centre, Germany.

Table 3: Variation of ionospheric irregularities during the storm events.

Figures caption

Figure 1: Geographic location of the stations. The magenta lines indicate ±15 degree dip latitude while the brown line indicates the magnetic equator (dip = 0 degree).

Figure 2: Variations of SYM-H, IMF Bz, IEFy, H, Diono, Ddyn and ROTI over the crests and

trough of the African EIA from 21 – 26 April 2012. The broken vertical line indicates the time of sudden storm commencement. In panel 4, the light blue area represents the limit of day-by-day variation of H, the tick blue line is the regular variation of H while the red line is the observed H.

Figure 3: Variations of SYM-H, IMF Bz, IEFy, H, Diono, Ddyn and ROTI over the crests and trough of the African EIA from 13 – 18 July 2012. The broken vertical line indicates the time of sudden storm commencement. In panel 4, the light blue area represents the limit of day-by-day variation of H, the tick blue line is the regular variation of H while the red line is the observed H.
Figure 4: Variations of SYM-H, IMF Bz, IEFy, H, Diono, Ddyn and ROTI over the crests and trough of the African EIA from 10 – 17 November 2012. The broken vertical line indicates the time of sudden storm commencement. In panel 4, the light blue area represents the limit of day-by-day variation of H, the tick blue line is the regular variation of H while the red line is the observed H.

Figure 5: Variations of SYM-H, IMF Bz, IEFy, H, Diono, Ddyn and ROTI over the crests and trough of the African EIA from 16 – 21 March 2013. The broken vertical line indicates the time of sudden storm commencement. In panel 4, the light blue area represents the limit of day-by-day variation of H, the tick blue line is the regular variation of H while the red line is the observed H.

Figure 6: Variations of SYM-H, IMF Bz, IEFy, H, Diono, Ddyn and ROTI over the crests and trough of the African EIA from 25 – 30 June 2013. The broken vertical line indicates the time of sudden storm commencement. In panel 4, the light blue area represents the limit of day-by-day variation of H, the tick blue line is the regular variation of H while the red line is the observed H.

Figure 7: Variations of SYM-H, IMF Bz, IEFy, H, Diono, Ddyn and ROTI over the crests and trough of the African EIA from 17 – 23 February 2014. The broken vertical line indicates the time of sudden storm commencement. In panel 4, the light blue area represents the limit of day-by-day variation of H, the tick blue line is the regular variation of H while the red line is the observed H.

Figure 8: Variations of SYM-H, IMF Bz, IEFy, H, Diono, Ddyn and ROTI over the crests and trough of the African EIA from 16 – 21 March 2015. The broken vertical lines indicate the time

of arrival of the shock. In panel 4, the light blue area represents the limit of day-by-day variation of H, the tick blue line is the regular variation of H while the red line is the observed H.

Figure 9: Effects of PPEFs over the African longitude (30^{o}E) during the main phase of the storm of (a) 23 April 2012, (b) 15 July 2012, (c) 13 November 2013, (d) 17 March 2013, (e) 28 June 2013, (f) 19 February 2014 and (g) 17 March 2015.

Table 1: Coordinates of the GPS and magnetometer stations

S/N	**Station / Country**	**Station code**	**Geo. Lat. GLAT**	**Geo. Long GLON**	**Mag. lat. (MLAT)**
		GPS station			
1	Nama, Saudi Arabia	nama	19.21^{0}N	42.05^{0}E	11.49^0
2	Sheb, Eritrea	sheb	15.85^{0}N	39.05^{0}E	7.36^0
3	Asab, Eritrea	asab	13.06^{0}N	42.65^{0}E	4.91^0
4	Addis Ababa, Ethiopia	adis	9.03^{0}N	38.77^{0}E	0.16^0
5	Eldoret, Kenya	moiu	0.29^{0}N	35.29^{O}E	-9.17^0
6	Kigali, Rwanda	nurk	1.94^{0}S	30.09^{0}E	-11.62^0
7	Malindi, Kenya	mal2	2.99^{0}S	40.19^{0}E	-12.42^0
		Magnetometer station			
	Addis Ababa, Ethiopia	AAE	9.03^{0}N	38.77^{0}E	0.16^0

Table 2: Magnetic quietest days during each storm. These are five international quietest days provided by GFZ, Helmholtz Postdam Centre, Germany.

	Storm events						
Quiet day designation	April 2012	July 2012	November 2012	March 2013	June 2013	February 2014	March 2015
Q1	30	13	09	08	16	13	10
Q2	06	26	30	07	26	26	30
Q3	09	27	28	26	17	14	05
Q4	08	18	04	25	13	25	14
Q5	16	31	11	13	14	02	09

Table 3: Variation of ionospheric irregularities during the storm events

Storm	SYM H (nT)	Electric current (H Adis) (UT)	Irregularities over Northern crest (UT)	Irregularities over Trough (UT)	Irregularities over Southern crest (UT)
April 24 2012	-124 nT	23 Apr: Westward (1630-1800) Eastward (1800-1830) 24 & 25 Apr: Westward	Inhibited for 1h30min Short triggering Inhibited on 24-25	Inhibited for 1h30min Weak irregularities Inhibited on 24-25	Inhibited for 1h30min Short triggering Inhibited on 24-25
July 15 2012	-118 nT	14 Jul: Westward (1800-2100) 15 -16 Jul: Westward 17 Jul: Westward	Reduction 1800-2100; Absent on 15-16 Present on 17	Inhibited 1800-2400 Absent on 15-16 Jul Absent on 17 Jul	Reduction 1800-2100; Absent on 15-16 till 2130. Present on 17
November 13-14 2012	-114 nT	14 Nov: Westward (0200-2400) 15-16 Nov: Westward (06:00-17:00)	Absent on 14 & 16 Nov Present on 15& 17 Nov	Absent on 14 -17 Nov	Absent on 14 & 16 Nov Present on 15& 17 Nov
March 17 2013	-132 nT	17 Mar: Eastward (1400-2100) 18 Mar: Westward 19 Mar: No disturbed current 20 Mar: Westward (2030-2400)	Triggering (1700-1800) Absent on 18 Mar Absent on 19 Mar Absent on 20 Mar	Triggering (1700-1800) Absent on 18 Mar Absent on 19 Mar Absent on 20 Mar	Triggering (1700-1800) Absent on 18 Mar Present (1900-2200) Absent on 20 Mar
June 29 2013	-104 nT	28-29 Jun: Westward	Absent (1800-2400)	Absent(1800-2400)	Present (2100-2400)
February 19 2014	-127 nT	19 Feb: Westward (1400-1900) 20 Feb: Eastward(18:16 UT)/ Westward 21-22 Feb: Westward	Absent on 19 Feb Triggering (1800-2030) Absent (1700-2100)	Absent on 19 Feb Triggering (1800-2030) Absent (1700-2100)	Absent on 19 Feb Triggering (1800-2030) Absent (1700-2100)
March 17 2015	-228 nT	17 to 19 Mar: Westward	Inhibited on 17 to 19 Mar	Inhibited on 17 to 19 Mar	Inhibited on 17 to 19 Mar

Figure 1.

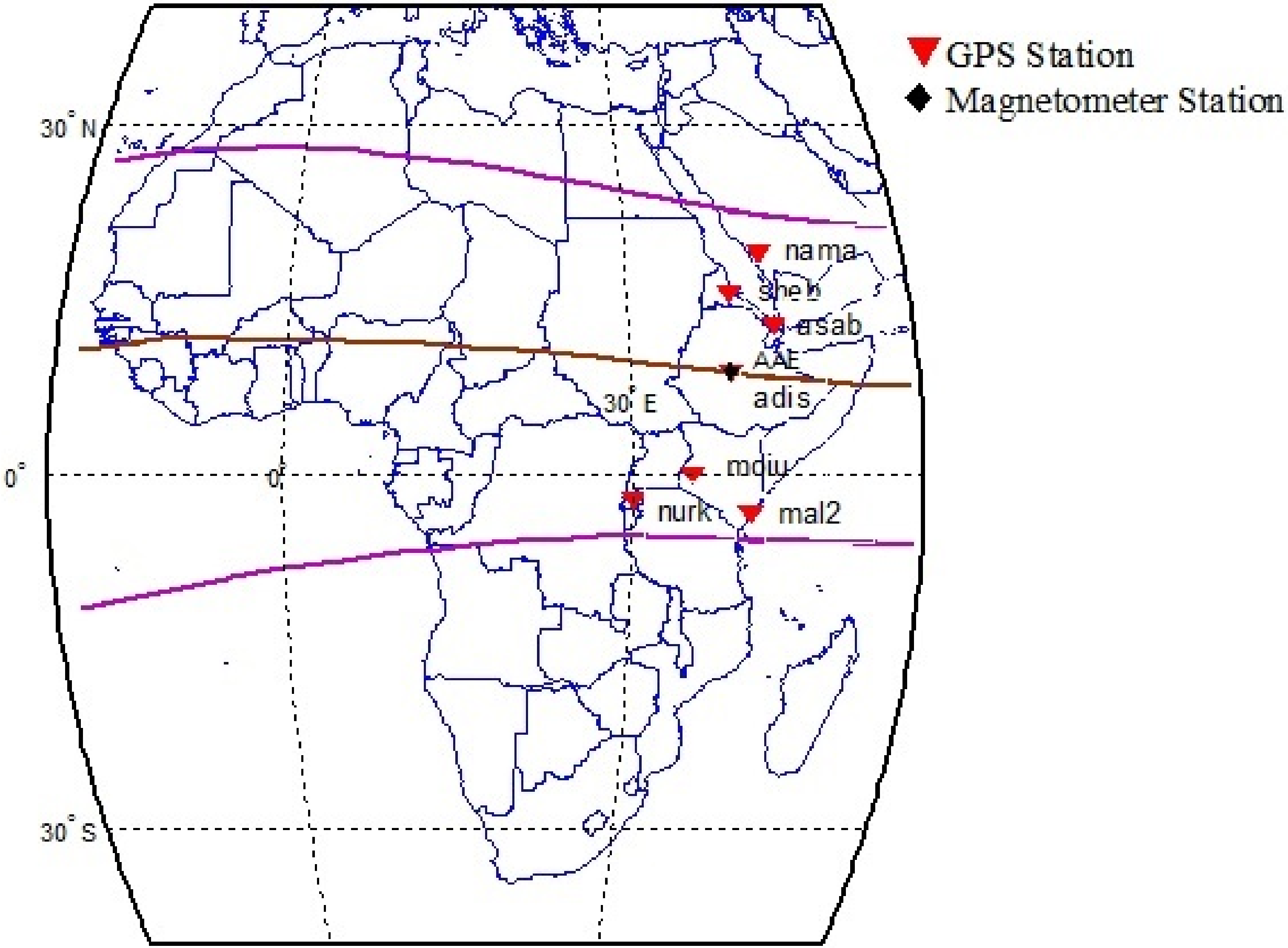
GPS Station
Magnetometer Station
30° N
0°
30° S
0°
30° E
nama
sheb
asab
AAE
adis
mdiu
nurk
mal2

Figure 2.

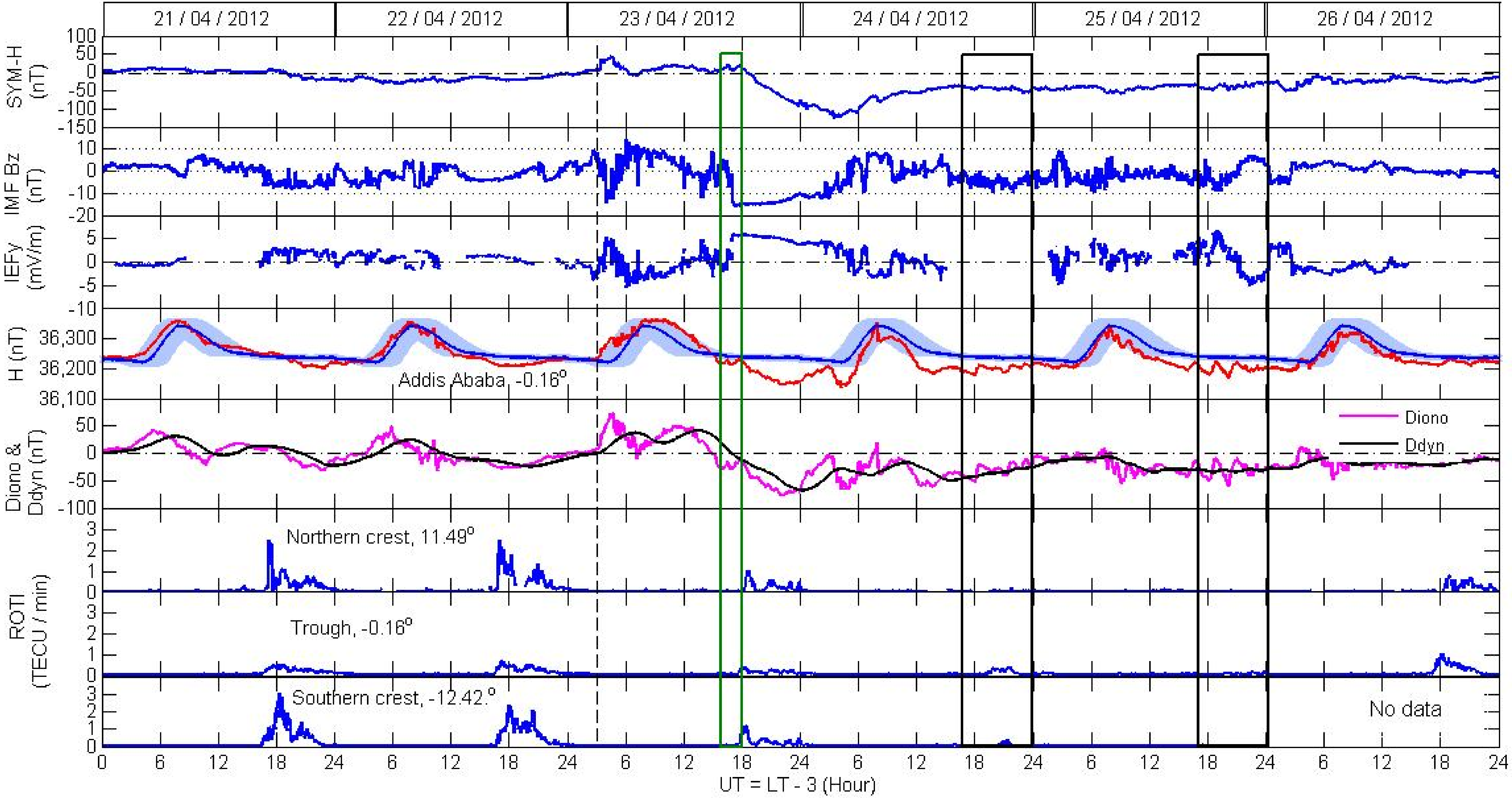

21 / 04 / 2012
22 / 04 / 2012
23 / 04 / 2012
24 / 04 / 2012
25 / 04 / 2012
26 / 04 / 2012
SYM-H (nT)
IMF Bz (nT)
IEFy (mV/m)
H (nT)
Addis Ababa, -0.16°
Diono & Ddyn (nT)
Diono
Ddyn
ROTI (TECU / min)
Northern crest, 11.49°
Trough, -0.16°
Southern crest, -12.42.°
No data
UT = LT - 3 (Hour)

Figure 3.

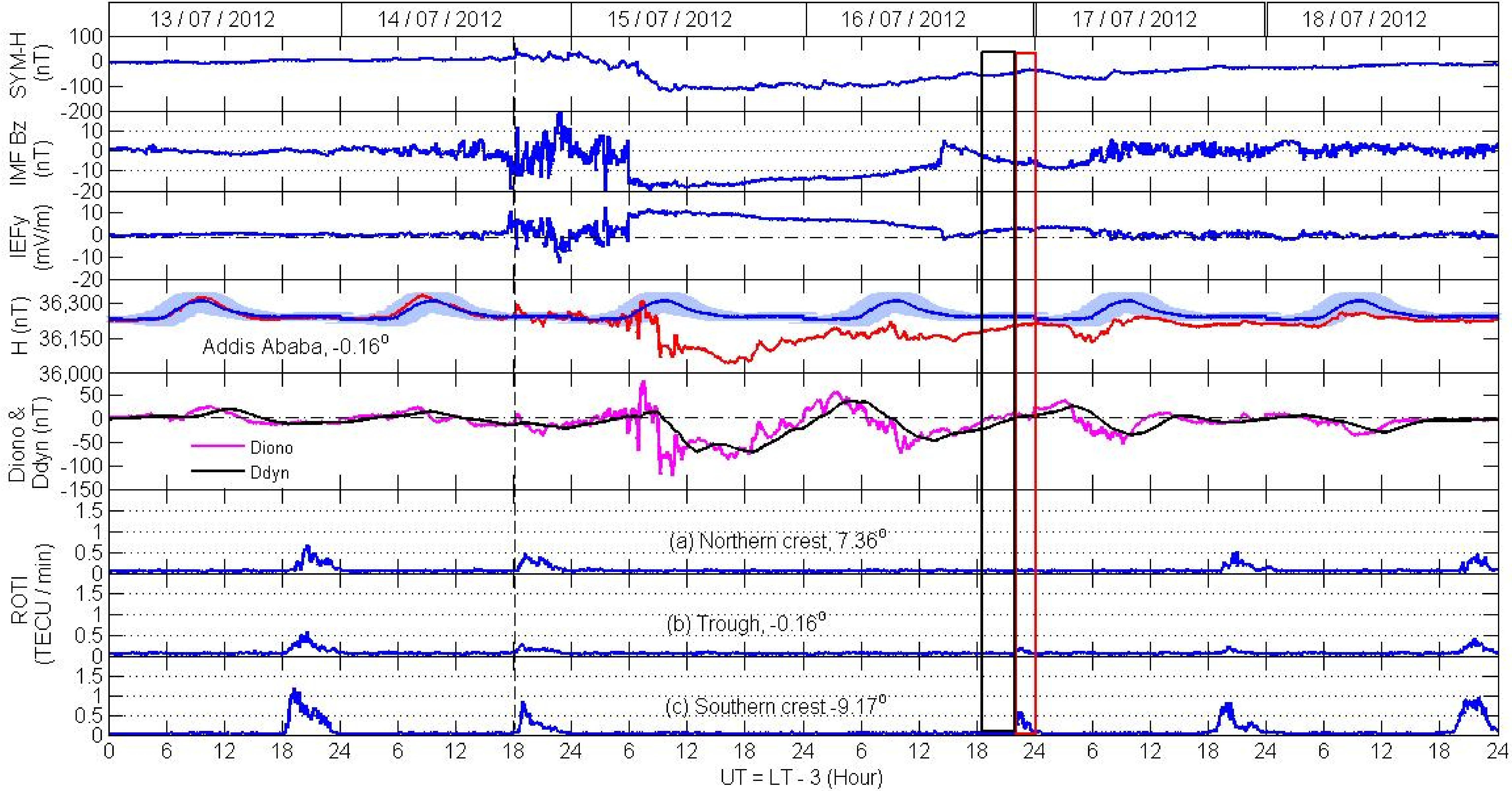

13 / 07 / 2012
14 / 07 / 2012
15 / 07 / 2012
16 / 07 / 2012
17 / 07 / 2012
18 / 07 / 2012
SYM-H (nT)
IMF Bz (nT)
IEFy (mV/m)
H (nT)
Addis Ababa, -0.16°
Diono & Ddyn (nT)
Diono
Ddyn
(a) Northern crest, 7.36°
ROTI (TECU / min)
(b) Trough, -0.16°
(c) Southern crest -9.17°
UT = LT - 3 (Hour)

Figure 4.

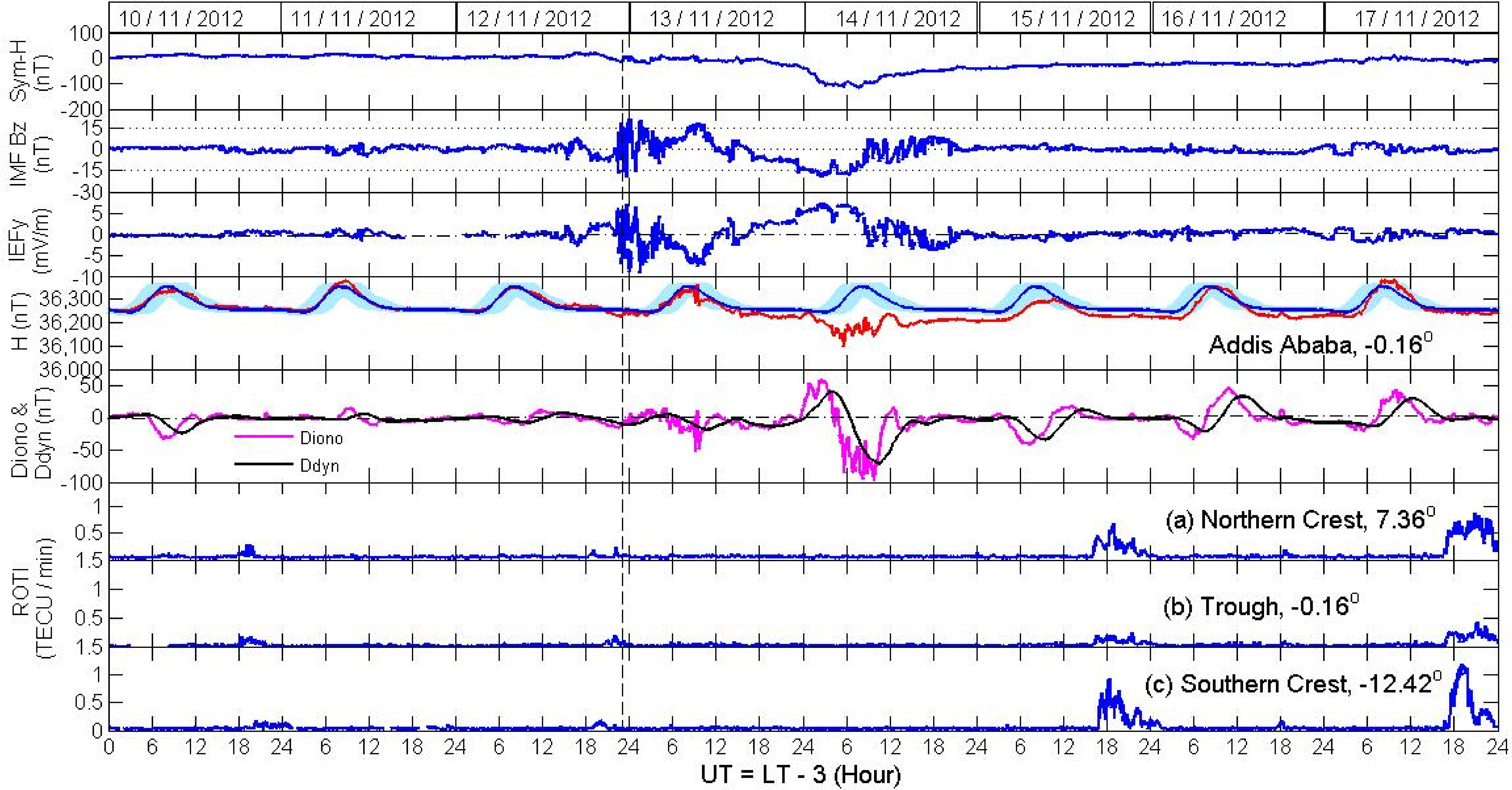

10 / 11 / 2012
11 / 11 / 2012
12 / 11 / 2012
13 / 11 / 2012
14 / 11 / 2012
15 / 11 / 2012
16 / 11 / 2012
17 / 11 / 2012
Sym-H (nT)
IMF Bz (nT)
IEFy (mV/m)
H (nT)
Addis Ababa, -0.16°
Diono & Ddyn (nT)
Diono
Ddyn
(a) Northern Crest, 7.36°
ROTI (TECU / min)
(b) Trough, -0.16°
(c) Southern Crest, -12.42°
UT = LT - 3 (Hour)

Figure 5.

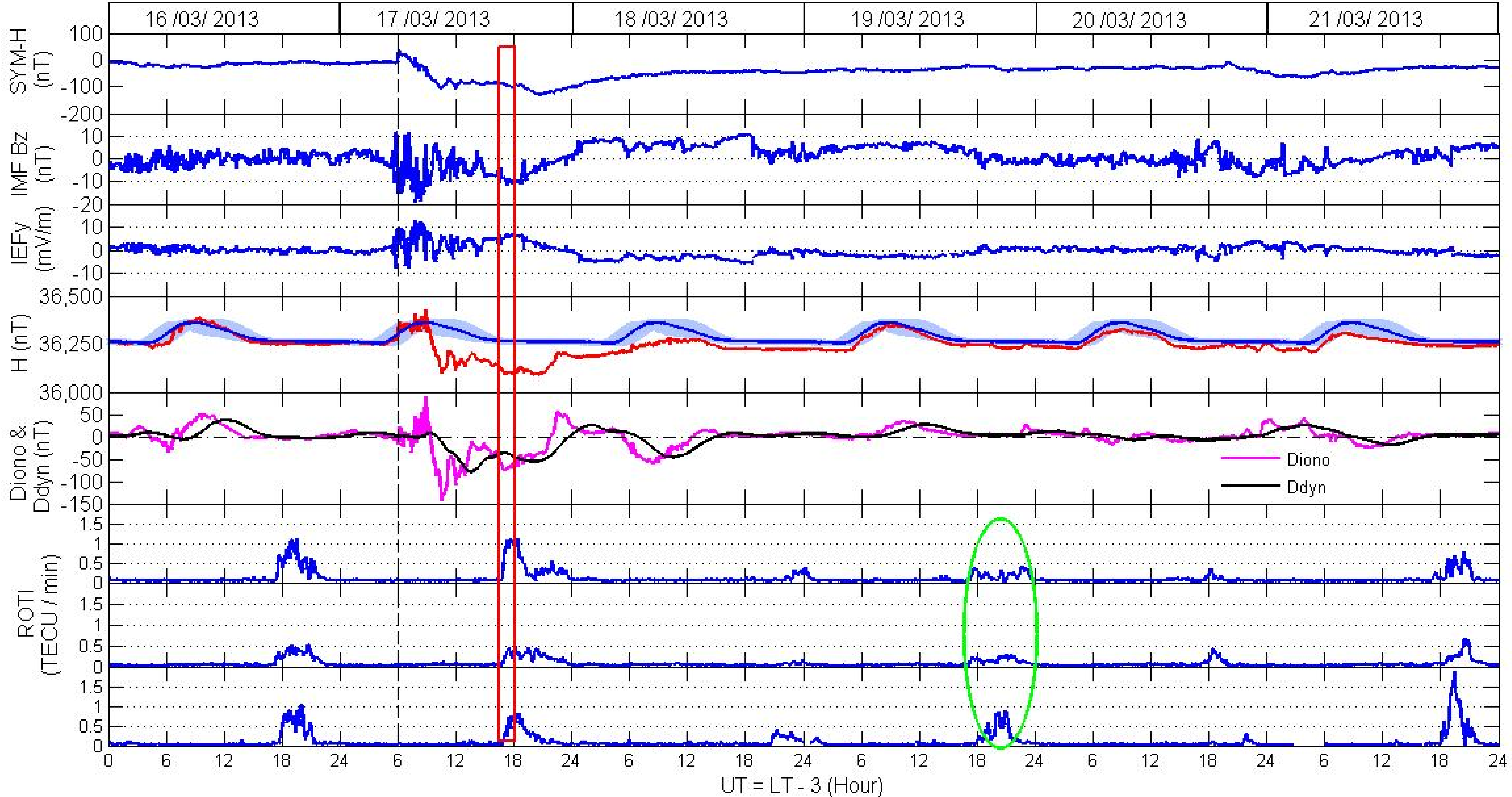

16 /03/ 2013
17 /03/ 2013
18 /03/ 2013
19 /03/ 2013
20 /03/ 2013
21 /03/ 2013
SYM-H (nT)
IMF Bz (nT)
IEFy (mV/m)
H (nT)
Diono & Ddyn (nT)
Diono
Ddyn
ROTI (TECU / min)
UT = LT - 3 (Hour)

Figure 6.

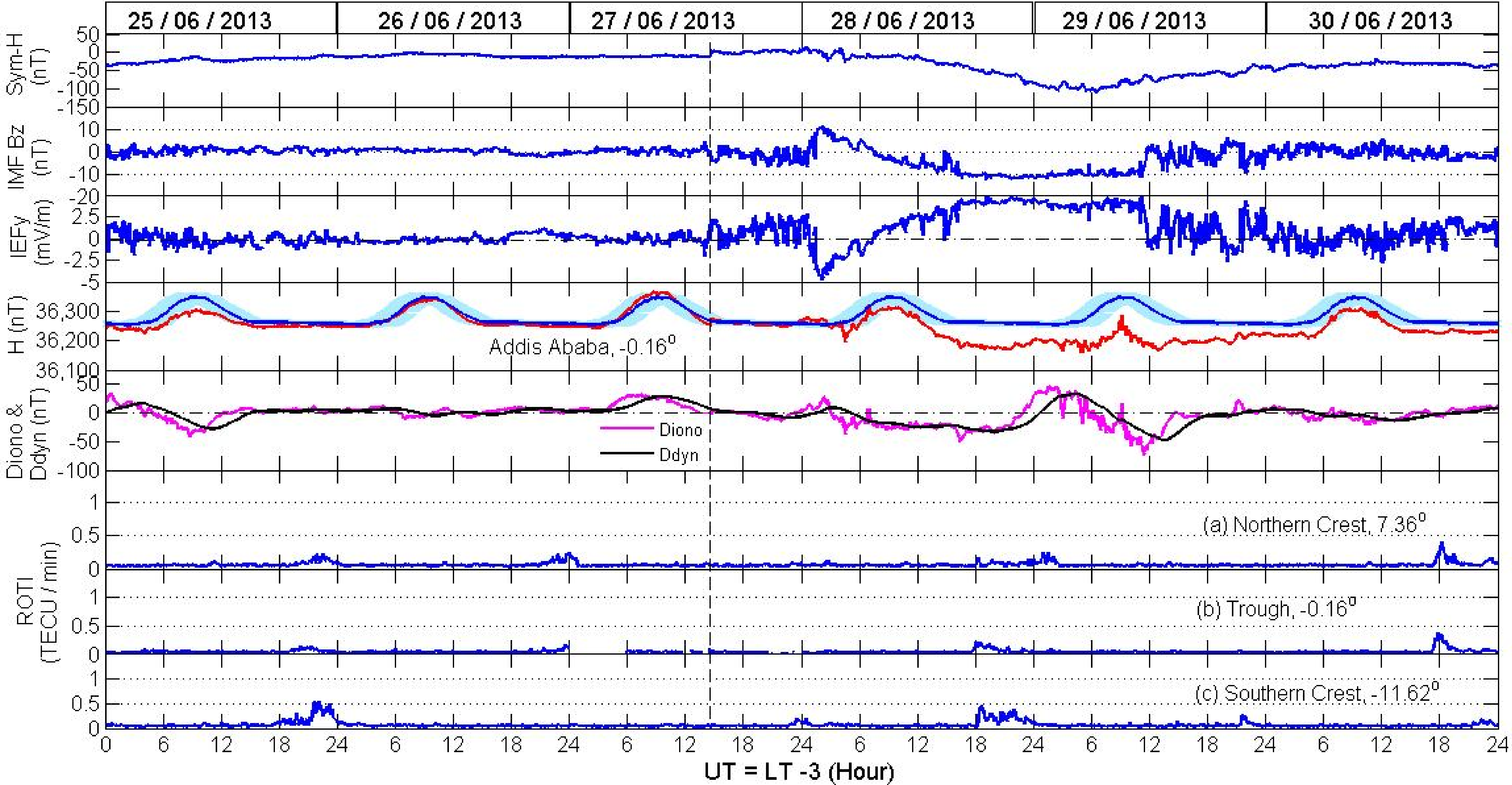

25 / 06 / 2013
26 / 06 / 2013
27 / 06 / 2013
28 / 06 / 2013
29 / 06 / 2013
30 / 06 / 2013
Sym-H (nT)
IMF Bz (nT)
IEFy (mV/m)
H (nT)
Addis Ababa, -0.16°
Diono & Ddyn (nT)
Diono
Ddyn
(a) Northern Crest, 7.36°
ROTI (TECU / min)
(b) Trough, -0.16°
(c) Southern Crest, -11.62°
UT = LT -3 (Hour)

Figure 7.

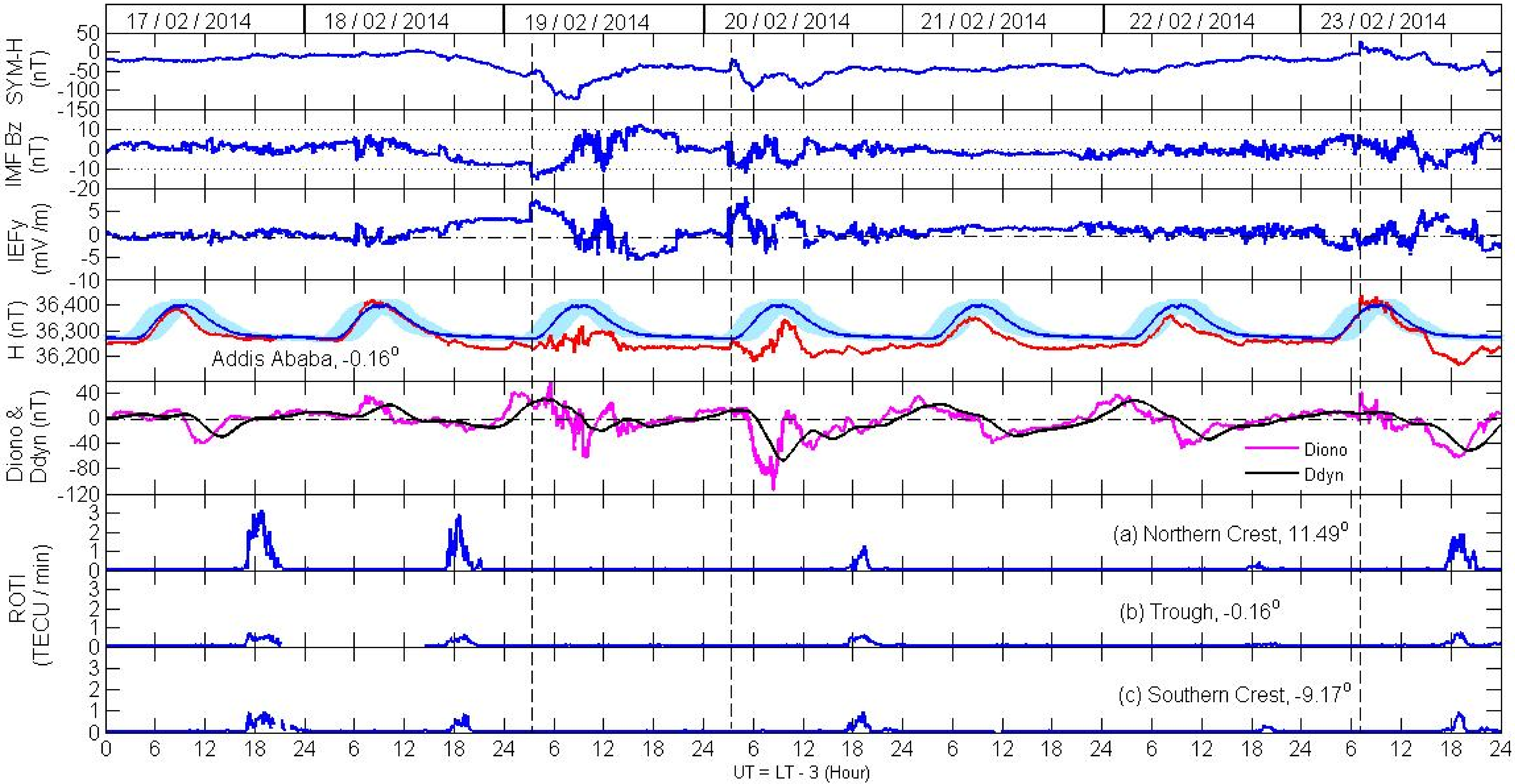
17 / 02 / 2014
18 / 02 / 2014
19 / 02 / 2014
20 / 02 / 2014
21 / 02 / 2014
22 / 02 / 2014
23 / 02 / 2014
SYM-H (nT)
IMF Bz (nT)
IEFy (mV /m)
H (nT)
Addis Ababa, -0.16°
Diono & Ddyn (nT)
Diono
Ddyn
ROTI (TECU / min)
(a) Northern Crest, 11.49°
(b) Trough, -0.16°
(c) Southern Crest, -9.17°
UT = LT - 3 (Hour)

Figure 8.

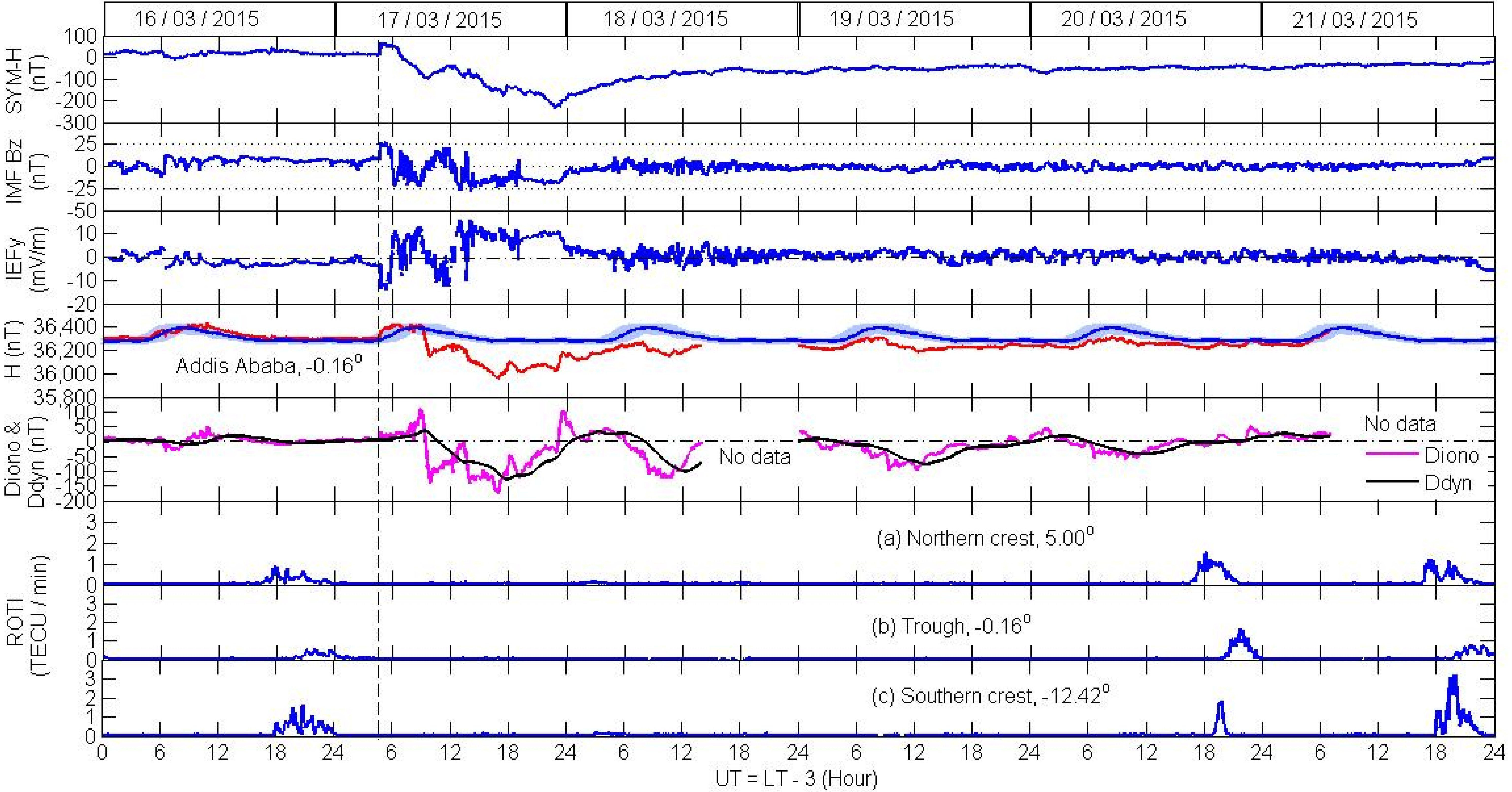
16 / 03 / 2015
17 / 03 / 2015
18 / 03 / 2015
19 / 03 / 2015
20 / 03 / 2015
21 / 03 / 2015
SYM-H (nT)
IMF Bz (nT)
IEFy (mV/m)
H (nT)
Addis Ababa, -0.16°
Diono & Ddyn (nT)
No data
No data
Diono
Ddyn
(a) Northern crest, 5.00°
ROTI (TECU / min)
(b) Trough, -0.16°
(c) Southern crest, -12.42°
UT = LT - 3 (Hour)

Figure 9.

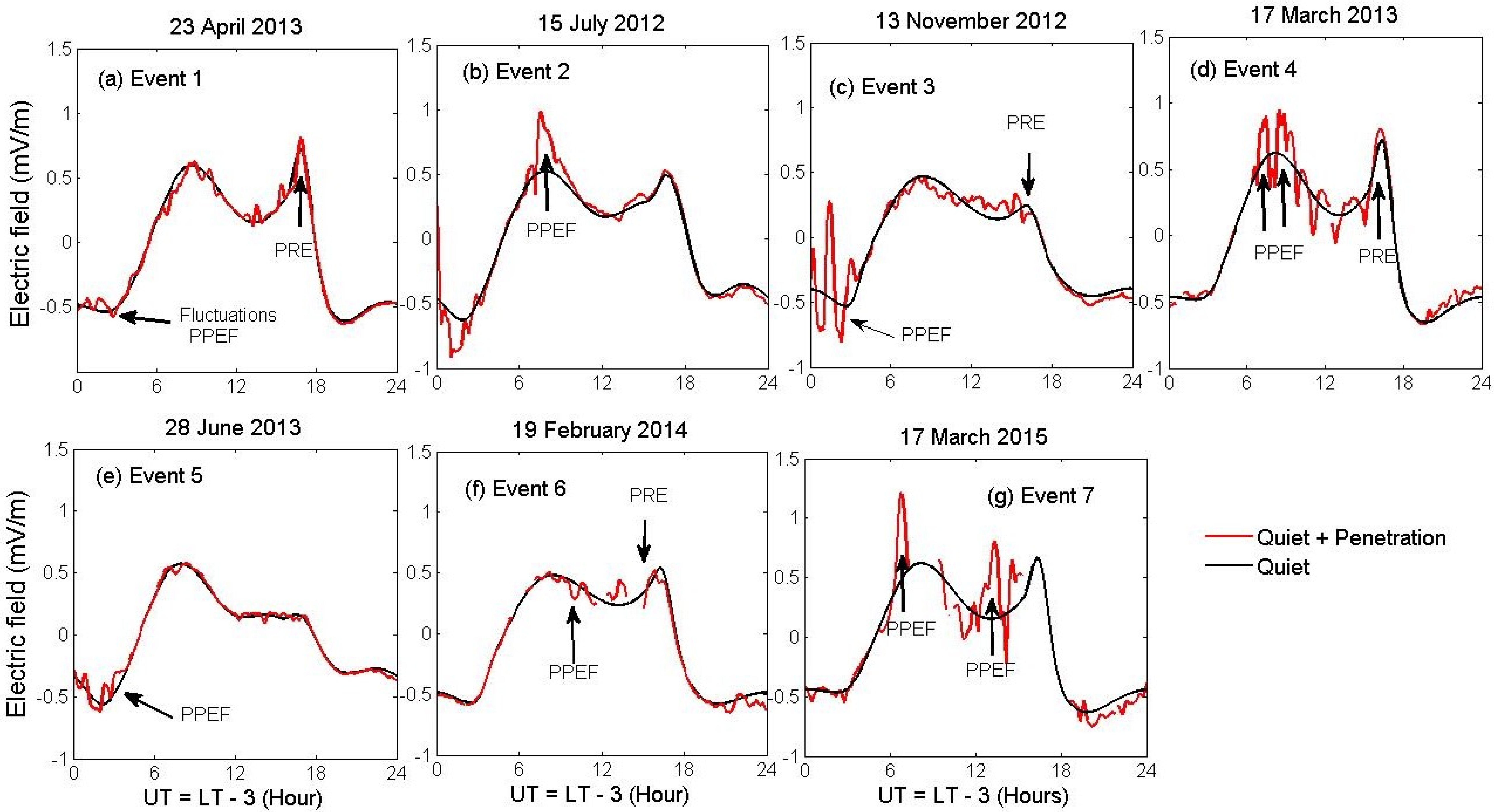
23 April 2013
(a) Event 1
PRE
Fluctuations
PPEF
15 July 2012
(b) Event 2
PPEF
13 November 2012
(c) Event 3
PRE
PPEF
17 March 2013
(d) Event 4
PPEF
PRE
28 June 2013
(e) Event 5
PPEF
19 February 2014
(f) Event 6
PRE
PPEF
17 March 2015
(g) Event 7
PPEF
PPEF
Electric field (mV/m)
UT = LT - 3 (Hour)
UT = LT - 3 (Hours)
Quiet + Penetration
Quiet